https://doi.org/10.5194/egusphere-2023-2641
Preprint. Discussion started: 8 February 2024

Measurement report: Source attribution and estimation of black carbon levels in an urban hotspot of the central Po Valley: An integrated approach combining high-resolution dispersion modelling and micro-aethalometers

Giorgio Veratti[1,2], Alessandro Bigi[2], Michele Stortini[3], Sergio Teggi[2], and Grazia Ghermandi[2]

[1]Department of Life Sciences. University of Modena and Reggio Emilia, 41125 Modena, Italy
[2]Department of Engineering 'Enzo Ferrari'. University of Modena and Reggio Emilia, 41125 Modena, Italy
[3]ARPAE, Regional Environmental Agency of Emilia-Romagna, 40122 Bologna, Italy

Correspondence: Giorgio Veratti (giorgio.veratti@unimore.it)

Abstract. Understanding black carbon (BC) levels and their sources in urban environments is of paramount importance due to their far-reaching health, climate and air quality implications. While several recent studies have assessed BC concentrations at specific fixed urban locations, there is a notable lack of knowledge in the existing literature on spatially resolved data alongside source estimation methods. This study aims to fill this gap by conducting a comprehensive investigation of BC levels and sources in Modena (Po Valley, Italy), which serves as a representative example of a medium-sized urban area in Europe. Using a combination of multi-wavelength micro-aethalometer measurements and a hybrid Eulerian-Lagrangian modelling system, we studied two consecutive winter seasons (February-March 2020 and December 2020-January 2021). Leveraging the multi-wavelength absorption analyser (MWAA) model, we differentiate sources (fossil fuel combustion, FF, and biomass burning, BB) and components (BC vs. brown carbon, BrC) from micro-aethalometer measurements. The analysis reveals consistent, minimal diurnal variability in BrC absorption, in contrast to FF-related sources, which exhibit distinctive diurnal peaks during rush hours, while BB sources show less diurnal variation. The city itself contributes significantly to BC concentrations (52% ± 10%), with BB and FF playing a prominent role (35% ± 15% and 9% ± 4%, respectively). Long-distance transport also influences BC concentrations, especially in the case of BB and FF emissions, with 28% ± 1% and 15% ± 2%, respectively. When analysing the traffic related concentrations, Euro 4 diesel passenger cars considerably contribute to the exhaust emissions. These results provide valuable insights for policy makers and urban planners to manage BC levels in medium-sized urban areas, taking into account local and long-distance sources.

1 Introduction

Both black carbon (BC) and elemental carbon (EC) are carbonaceous particles associated with particulate matter (PM) that result from incomplete combustion processes and have light-absorbing properties. Although they are commonly mistaken for synonyms, these two terms should not be treated as completely interchangeable. The vocabulary associated with BC is extensive and many uncertainties arise from the definitions and measurement methods used for BC (Petzold et al., 2013; Bond

https://doi.org/10.5194/egusphere-2023-2641
Preprint. Discussion started: 8 February 2024

et al., 2013; Grange et al., 2020). According to the recommendations of Petzold et al. (2013), BC is the preferred term when formally characterising a material that is ideally light absorbing and composed predominantly of carbon. Conversely, EC is a pure form of carbon, consisting only of carbon atoms not bonded to other elements, and this term should be used instead of BC when reporting data derived from methods that specifically measure the carbon content of carbonaceous matter. While these formal definitions strive for rigour, their practical application can be challenging due to the inherent variability of carbonaceous matter. Unlike pure substances, real-world BC exists as a complex mixture of various compounds with different properties. For this reason, a common approach to defining BC is based on properties such as light absorption, solubility, thermal stability, morphology or microstructure (Petzold et al., 2013).

BC originates from a variety of sources, including combustion engines (especially diesel), residential burning of wood and coal, field burning of agricultural residues, as well as forest and vegetation fires. The detrimental consequences associated with BC have become a key element of scientific investigation and public concern, necessitating a comprehensive understanding of its sources, behaviour, and potential mitigation strategies. The adverse effects of BC on human health are well-documented in the literature. Inhalation of BC particles has been linked to various respiratory and cardiovascular conditions, including asthma, chronic bronchitis, reduced lung function, and increased risk of heart attacks and strokes (Song et al., 2022; Janssen et al., 2012; Grahame et al., 2014; Rohr and McDonald, 2016; Janssen et al., 2011). Moreover, long-term exposure to BC has been associated with an elevated incidence of lung cancer (Chang et al., 2022). These health risks are particularly worrisome considering the widespread prevalence of BC in urban areas (Reche et al., 2011; Ali et al., 2021) and its ability to penetrate deep into the respiratory system (Saputra et al., 2014; Tang et al., 2020), posing a significant threat to vulnerable populations, such as children, the elderly, and individuals with pre-existing respiratory disorders.

BC not only poses adverse health effects but also exerts significant impacts on the Earth's radiation balance through various mechanisms (Chung and Seinfeld, 2005; Wang, 2004; Roberts and Jones, 2004). These include direct and indirect effects, altering the amount, distribution, and properties of solar energy. The direct effects encompass the absorption and scattering of sunlight by BC, leading to localised atmospheric warming and influencing the distribution of solar radiation within the atmosphere (Menon et al., 2002; Ramanathan et al., 2001; Ramanathan and Carmichael, 2008). Estimates of BC's direct radiative forcing range from +0.1 to +1.0 $\mathrm{W\,m^{-2}}$, exhibiting variations depending on the methodology employed, such as bottom-up emission inventory and atmospheric transport model approaches, or observation-based estimates (Wang et al., 2016; Bond et al., 2013). In addition to the direct effects, BC particles have indirect impacts on the Earth's radiation balance by interacting with clouds. BC can serve as cloud condensation nuclei (CCN) or ice nuclei (IN), influencing the formation of cloud droplets and ice particles (Hendricks et al., 2011; Koch et al., 2011). The presence of BC can modify cloud microphysical properties, including droplet size, concentration, cloud lifetime and precipitation processes. These indirect effects have been estimated to range from -0.13 to -0.11 $\mathrm{W\,m^{-2}}$, contributing to a negative radiative forcing (Cherian et al., 2017; Koch et al., 2011). Considering both the direct and indirect effects, the combined impact of BC on the Earth's radiation balance results in a positive radiative forcing on the climate system, exacerbating global warming and climate change.

In the literature, several approaches have been employed to measure BC, EC or more generally light-absorbing aerosols. These approaches can be categorised into four main methods: thermo-optical determination, photothermal interferometry, pho-

https://doi.org/10.5194/egusphere-2023-2641
Preprint. Discussion started: 8 February 2024

toacoustic spectroscopy and optical determination. Thermo-optical determination involves the measurement of light-absorbing aerosols by analysing their thermal properties. The technique typically relies on heating the sample in a controlled environment and measuring the resulting changes in optical properties, such as light absorption and scattering, as a function of temperature. By observing these changes, one can estimate the amount and type of light-absorbing aerosols present in the sample (Chow et al., 2007; Bauer et al., 2009; Brown et al., 2019). Field experiments adopting this determination method are for example Merico et al. (2019); Liakakou et al. (2020); Bigi et al. (2017).

Photo-thermal interferometry is a technique that combines laser-induced heating with interferometric measurements to quantify light-absorbing aerosols (Lee and Moosmüller, 2020; Visser et al., 2023; Li et al., 2016). By directing a laser beam onto the aerosol sample, the absorbed light generates local temperature gradients, causing changes in the refractive index and thus altering the phase of a probe laser beam passing through the sample. These phase changes are then measured interferometrically to determine the concentration of light-absorbing aerosols. On the other hand, photo-acoustic methodologies involve the use of laser-induced acoustic waves to detect and quantify light-absorbing aerosols. In this technique, a pulsed laser is used to heat the sample, causing the aerosols to absorb the light and generate acoustic waves. By measuring the amplitude of these acoustic waves, the concentration of light-absorbing aerosols can be determined (Fischer and Smith, 2018; Petzold and Niessner, 1996; Guo et al., 2014). The deployment of photo-thermal and photo-acoustic instruments in field settings has been limited due to operational challenges, which has hindered the widespread adoption of these techniques. However, there has been a recent resurgence of interest in these methods with the development of a new generation of photometers and interferometers (Drinovec et al., 2022; Visser et al., 2020, 2023).

In addition to the aforementioned techniques, optical determination has gained popularity in recent years for measuring the light absorption properties of BC aerosols due to its cost-effectiveness, comparability with chemical analysis and ability to provide high temporal resolution results for real-time monitoring studies (Kaskaoutis et al., 2021a, b; Yus-Díez et al., 2021; Bernardoni et al., 2021). This approach utilises a light source, such as a spectrometer or a nephelometer, to quantify the amount of light absorbed or attenuated by the aerosols. By means of specific mass absorption efficiency (MAE; also known as the mass absorption cross section, MAC), the aerosol light absorption coefficient can then be converted into the light-absorbing carbon mass concentration. Although this relationship is simple, the value of MAE varies considerably in time and space depending on the emission sources, transport phenomena, combustion conditions, particle ageing and mixing state (Chan et al., 2011; Mbengue et al., 2021), making the conversion process a source of potential uncertainty (Petzold et al., 2013). When considering BC material, the term equivalent BC (eBC) is commonly used to report the mass concentration indirectly determined by light absorption techniques such as filter-based absorption photometers (Petzold et al., 2013). Therefore, the term eBC will be used throughout this study to refer to those calculated using filter-based absorption photometers.

BC exhibits distinctive light absorption characteristics, particularly in the infrared range, facilitating its identification and quantification. Widely used instruments exploiting this technique are the aethalometer, such as the AEs models (e.g. AE31, AE33, AE36 and AE43, Magee Scientific Co.) or the portable micro-aethalometer MA series (e.g. MA200, MA300 and MA350, Aethlabs) which are filter-based optical instruments operating at different wavelengths. This later feature, coupled with the

https://doi.org/10.5194/egusphere-2023-2641
Preprint. Discussion started: 8 February 2024

usage of source-specific absorption Ångström exponent, can be used for the source apportionment of black carbon (Zotter et al., 2017; Sandradewi et al., 2008; Massabò et al., 2015; Bernardoni et al., 2017b).

Source apportionment of BC is essential to gain insight into the specific pollution sources contributing to atmospheric concentrations. This analysis enables the development of targeted mitigation strategies, in line with the recommendation proposed by the EU legislation (European Council, 2008), which highlights the importance of identifying and addressing specific emission source sectors to effectively reduce air pollution. Furthermore, the World Health Organization (WHO), in its recently updated global air quality guidelines, has recommended the systematic measurement of BC (or EC), the establishment of BC inventories and, where appropriate, the implementation of BC reduction measures (WHO, 2021). This research aims to provide information on the levels of BC and to identify the main sources of BC in the urban environment of Modena, a city of about 200,000 inhabitants located in the middle of the Po Valley, a densely populated and industrialised region in northern Italy, known for its high levels of air pollution (Bigi and Ghermandi, 2016; Bigi et al., 2012; Lonati et al., 2017; Perrino et al., 2014; Veratti et al., 2023; Thunis et al., 2021).

Previous studies have investigated the sources and transport of particulate matter in the Po valley using both chemical transport models (CTMs) and aerosol composition, such as for example Scotto et al. (2021); Paglione et al. (2020); Bernardoni et al. (2011); Pepe et al. (2019); Belis et al. (2019); Bernardoni et al. (2017a), but there is still a knowledge gap regarding the contribution of different sources to BC concentrations. For instance, a study by Mousavi et al. (2019) combined the usage of aethalometer, thermo-optical instruments and ^{14}C analysis to apportion between fossil fuel and biomass burning for three sites in the urban area of Milan and its surrounding. Similar studies in the Po valley have been conducted employing a variety of instruments such as aethalometers, Multi-Angle Absorption Photometers (MAAP), polar-photometers, and independent measurement of levoglucosan (Bernardoni et al., 2021; Massabò et al., 2015; Bernardoni et al., 2017b; Gilardoni et al., 2020). In addition, concerns about health effects have led recently to a surge of research in urban areas, highlighting eBC concentrations as a fundamental tracer of pollution in cities (Segersson et al., 2017; Pani et al., 2020). As a result, several studies have investigated the variability of eBC mass concentrations and the associated source apportionment at multiple urban locations. Examples of this research in Europe are Savadkoohi et al. (2023); Liakakou et al. (2020); Grange et al. (2020); Helin et al. (2018); Minderytė et al. (2022); Titos et al. (2017); Singh et al. (2018). Although all these studies utilised accurate methods for eBC determination and source apportionment, their results were limited to specific monitoring sites, including rural or urban background locations. As a consequence, they were unable to provide continuous spatial information across the entire city, which is an important information for consistent epidemiological analysis.

In addition to the aforementioned studies, other researchers have conducted modelling studies at the European level to assess the performance of air quality models in reproducing carbonaceous aerosol concentrations and their absorption properties, such as Mircea et al. (2019); Curci et al. (2019). Other works aimed at estimating BC concentrations at street level in small neighbourhoods of Paris, Brussels or Maribor using a state-of-art multi-scale modelling system, Street-in-Grid (Lugon et al., 2021) or a more simplified approach (Brasseur et al., 2015; Ježek et al., 2018). However, none of these studies focused on assessing total BC concentrations over an entire urban area at high resolution or attempted to apportion the sector-specific contribution.

https://doi.org/10.5194/egusphere-2023-2641
Preprint. Discussion started: 8 February 2024

In this study, we conducted a two-sampling period campaign during wintertime (February-March 2020 and between December 2020 and January 2021) in Modena, deploying two MA200 multi-wavelength micro-aethalometers at distinct urban locations, at traffic and background sites. The primary objectives were to determine total BC concentrations at both sites and to investigate the potential sources contributing to the observed concentrations. To support the identification of local and regional sources and to provide spatial information about BC concentrations, we employed a hybrid Lagrangian-Eulerian modelling system composed by GRAMM-GRAL (Oettl, 2015b, a, c) and the NINFA (Network dell'Italia del Nord per previsioni di smog Fotochimico e Aerosol, Vitali et al. (2023)) modelling suite, which is built upon the CHIMERE chemical transport model (Mailler et al., 2017; Menut et al., 2021). By combining observed and modelled data, we aimed to improve our understanding of the main emission sectors contributing to total BC levels for the development of effective mitigation strategies and to provide valuable insights for addressing environmental and health concerns related to BC.

The paper is structured as follows: section 2 provides an overview of the measurement campaign and the models that make up the hybrid system. Further details on the emission estimation are given in subsection 2.5. Section 3 presents the statistical metrics used to validate the model performance against the observational data. Section 4 presents the results of the measurement campaign and modelling activities. Finally, section 5 presents some concluding remarks.

2 Materials and methods

2.1 Sampling sites and measurement description

The measurement campaign was carried out in Modena, a medium-sized city in the Emilia-Romagna region of northern Italy. Modena is located about 50 kilometres south of the Po River, in the Po Valley, an area known for its dense population and industrialisation. The city, like the whole valley, has a continental climate with marked seasonal variations. In particular, during the winter months, the Po Valley has specific meteorological characteristics, such as stable atmospheric conditions and frequent low wind speeds, which contribute to the occurrence of thermal inversions. These atmospheric phenomena can hinder the dispersion of air pollutants in the region, as reported by many studies, such as Bigi et al. (2012); Pernigotti et al. (2012a, b); Ghermandi et al. (2017). In addition, the Po Valley is geographically bounded by the Apennines to the south and the Alps to the north, which act as natural barriers that further limit the movement of pollutants. As a result, the combination of high traffic volumes, industrial activities and the large number of densely populated urban areas in the valley can lead to the accumulation of pollutants.

In this study, aerosol measurements were performed using two MA200 micro-aethalometers (microAeth® MA Series, Aethlabs, USA) equipped with PTFE filter tapes. These instruments quantify the absorption of light-absorbing carbonaceous aerosols at five different wavelengths (375, 470, 528, 625 and 880 nm), allowing for the estimation of eBC concentrations by employing wavelength-specific mass absorption efficiencies (MAE).

Sampling was performed at two air quality monitoring stations in the city, utilising the existing glassware manifold inlet lines used for reactive gas monitors. The inlet temperature was maintained at 30 ± 2 °C and no size cut-off was applied to the aerosol particles entering the devices. One station is located in a public park on the west side of the city, representing typical

https://doi.org/10.5194/egusphere-2023-2641
Preprint. Discussion started: 8 February 2024

background conditions where pollution levels are influenced by a mixture of contributions rather than a single source type, while the other station is located in an urban traffic area characterised by high vehicular activity, serving as a representative location for areas of dense traffic and associated air pollution. The locations of the two stations are shown in Figure 1.

Throughout the study, the instruments operated at a flow rate of 100 mlmin^{-1} in dual-spot sampling mode to compensate for filter loading effects (Drinovec et al., 2015). Although several papers in the literature have emphasised the need for a multi-instrument approach to determine the multi-scattering correction factor (C_{ref}) for aethalometer filters (Bernardoni et al., 2021; Yus-Díez et al., 2021; Ferrero et al., 2021), with photothermal interferometry being recently identified as a suitable technique to provide a reference measurement of this parameter (Drinovec et al., 2022), this study lacked multi-instrument co-location. As a result, a constant C_{ref} of 1.3 was chosen to account for multiple light scattering within the filter fibres and between deposited particles and the filter, as suggested by the manufacturer (Aethlabs, 2024). To support this decision, a recent instrument intercomparison performed at an urban background site in Athens (Stavroulas et al., 2022) showed limited differences between the MA200 instrument set with C_{ref} of 1.3 and a MAAP (linear slope of 1.00 in winter and 1.07 in summer, with an r^2 of 0.92 for both the seasons). Furthermore, as site-specific MAE values for Modena were not available, we relied on the wavelength-specific values provided in the reference manual and reported in Table S1 in the supplement.

Measurements at the urban traffic site were made during two periods: from 4 February to 7 March 2020 and from 26 December 2020 to 21 January 2021, with a time resolution of 1 minute, while the background site was monitored from 4 February to 7 March 2020 with a time resolution of 1 minute and from 26 December 2020 to 7 January 2021 with a time resolution of 5 minutes. To account for occasional low absorption readings at the background site, the 1-minute data at the urban background location were aggregated to 5 minutes using the dual-spot compensation algorithm implemented in the R language (Bigi et al., 2023) following the formulation proposed by Drinovec et al. (2015). The MA200 measurements were evaluated based on the instrument's reported status, and flow calibration was performed before each filter change.

Strict lockdown measures were implemented in Northern Italy due to the SARS-CoV-2 pandemic from 8 March 2020 to 4 May 2020. Therefore, the winter data presented in this study represent a business-as-usual scenario, spanning across two winter seasons. Prior to the analysis, the concentration data were averaged to 1 hour to match the time resolution of observed meteorological variables and align with the typical time step used in modelling applications at urban and regional scales.

Absorption measurements from the MA200 devices were further partitioned into specific components, including BC, BrC (hereafter noted as b_{abs}^{BC} and b_{abs}^{BrC}) and their respective sources, namely fossil fuel (FF) and biomass burning combustion (BB), referred to $b_{abs,BC}^{FF}$ and $b_{abs,BC}^{BB}$, respectively. This partitioning was achieved using the Multi-Wavelength Absorption Analyzer model (MWAA) developed by Massabò et al. (2015); Bernardoni et al. (2017b). The MWAA model assumes that the Absorption Ångström Exponent (α), as defined by Moosmüller et al. (2009), is equivalent for BC and fossil fuel sources, while biomass burning is considered as the only source of BrC. Under these assumptions, the model holds that the total absorption at each wavelength adheres to the following equations:

$$b_{\mathrm{abs}} = b_{\mathrm{abs}}^{\mathrm{BC}}(\lambda) + b_{\mathrm{abs}}^{\mathrm{BrC}}(\lambda) = \mathrm{A} \cdot \lambda^{-\alpha^{\mathrm{BC}}} + \mathrm{B} \cdot \lambda^{-\alpha^{\mathrm{BrC}}} \quad (1)$$

https://doi.org/10.5194/egusphere-2023-2641
Preprint. Discussion started: 8 February 2024

Table 1. Characteristics and locations of meteorological and air quality stations employed in this study.

Station name	label	Longitude (°)	Latitude (°)	sensor height (m)	Type
Campus - DIEF	CMP	10.95037	44.62832	10	Meteorology
Dexter - Arpae	DEX	10.91699	44.65639	40	Meteorology
Geophysical observatory	OSS	10.92981	44.64809	50	Meteorology
Policlinico	POL	10.94429	44.63580	40	Meteorology
S. Pietro Capofiume	SPC	11.62567	44.65467	- (soundings)	Meteorology
via Giardini	urban traffic	10.90572	44.63699	4	Air Quality
parco Ferrari	urban background	10.90731	44.65157	4	Air Quality

$$b_{\text{abs}} = b_{\text{abs}}^{\text{FF}}(\lambda) + b_{\text{abs}}^{\text{BB}}(\lambda) = \text{A}' \cdot \lambda^{-\alpha^{\text{FF}}} + \text{B}' \cdot \lambda^{-\alpha^{\text{BB}}} \quad (2)$$

In Equations 1 and 2 are defined with $\alpha^{\text{BC}} = \alpha^{\text{FF}} = 1$, which approximates the centre of the α probability density function (PDF) during the morning rush hour at the urban traffic site (Figure S1 in the Supplement), indicative of fresh uncoated BC particles, as shown by Liu et al. (2018). The α value for BrC was determined by a preliminary nonlinear fit of Eq. 2, with α^{BrC} treated as a free parameter (resulting in a mean $\alpha^{\text{BrC}} = 3.9$). $\alpha^{\text{BB}} = 2$ was set based on the upper tail of the α PDF calculated from the fit over the five wavelength and applying a stringent filter of $r^2 > 0.99$ (Figure S1), as suggested for example by Tobler et al. (2021). The same value also aligns with the existing literature data for the Po Valley (Costabile et al., 2017; Vecchi et al., 2018; Bernardoni et al., 2011). Parameters A and B were then derived for each sample by multi-wavelength fitting of 1 (with a fixed α^{BrC} value) and A' , B' by multi-wavelength fitting of Eq. 2. For a comprehensive understanding of the MWAA model, reference can be made to the works of Massabò et al. (2015) and Bernardoni et al. (2017b). In addition, for a more detailed information on the source and component assignment performed on the data used in this study, detailed information can be found in the companion study by Bigi et al. (2023). Meteorological variables essential for the reconstruction of the wind field by the GRAMM-GRAL model, including downward global radiation, wind speed and direction, were obtained from the meteorological network of the Osservatorio Geofisico di Modena (identified as CMP, OSS and POL stations) and from the monitoring network managed by the Regional Environmental Agency Arpae (represented by the DEX station). Table 1 shows the locations and characteristics of the stations used in this study, while Figure 1 shows their positions on a map. The table also includes information on the locations where soundings were carried out and subsequently used in this study, denoted by the SPC label.

https://doi.org/10.5194/egusphere-2023-2641
Preprint. Discussion started: 8 February 2024

2.2 The hybrid Eulerian-Lagrangian modelling system

In this study, one of the main objectives was to perform a spatial investigation of BC concentrations in the urban environment of Modena and to provide valuable information on source apportionment. To achieve this, we used a hybrid modelling approach based on two key components: the GRAMM-GRAL dispersion modelling suite, a state-of-the-art Lagrangian simulation system, and the NINFA modelling tool.

The GRAMM-GRAL suite was specifically selected for its ability to simulate the dispersion of emissions within the study area, taking into account the complex urban landscape with its various obstacles such as buildings and structures. On the other hand, NINFA played a crucial role in complementing the output of the Lagrangian model and providing additional insights into BC pollution. NINFA was used to estimate background concentrations from sources outside the urban area and to assess the influence of regional factors on BC levels in Modena. By integrating the strengths of both models, we aimed at a comprehensive understanding of BC concentrations in the study area, capturing the complex dynamics of BC transport in the urban environment. Furthermore, the Lagrangian models used in our approach offered the advantage of generating concentration fields specific to selected source emissions, allowing the estimation of source apportionment and providing valuable information on the contributions of different emission sectors to BC levels. To avoid duplication of emissions in Modena, the BC emission fluxes within the urban domain of interest were set to zero when using NINFA. In addition, BC was treated as an inert species in both models, leading to the exclusion of any chemical reactions involving BC. As a result, the total BC concentration was determined by combining the NINFA output, which represents the contribution of the external areas of Modena, with the GRAL output, which instead represents the contribution of the city. For a more complete understanding of the modelling system and the coupling between an Eulerian and a Lagrangian model used in this study, reference is made to previously published works such as Veratti et al. (2020, 2021), where a detailed description is provided.

2.3 NINFA set-up

Simulations were conducted using NINFA, a modelling system based on the state-of-the-art chemical transport model CHIMERE v2017r4 (Mailler et al., 2017) and operated by the Regional Agency for Prevention, Environment and Energy (ARPAE). This suite was employed to investigate surface concentrations of BC aerosol at the regional scale. The study area covered a significant part of the Po Valley, with a grid size of 114 x 86 cells. The grid extended from 8.78° E to 13.13° E longitude and from 43.57° N to 45.79° N latitude, with a fine horizontal resolution of 3 km (see Figure 1 for visualisation).The vertical grid consisted of 15 levels, ranging from 997 hPa (25 m) for the first layer to 500 hPa. This high-resolution grid was specifically chosen to accurately represent the spatial scale characteristic of regional air pollution in the area of interest, and it also allowed a precise delineation of the urban area of Modena, where urban emissions were excluded from the simulations. The meteorological input to NINFA was provided by the output of COSMO-2I, a limited domain atmospheric model used by the Italian National Civil Protection Agency and operated by the local environmental agency Arpae. The COSMO domain covers the Italian peninsula with a horizontal resolution of 2.2 km and 30 vertical levels ranging from 20 m to 22 km. Meteorological variables were spatially interpolated to the NINFA grid using the libsim libraries (Clima, 2023). The aerosol module imple-

https://doi.org/10.5194/egusphere-2023-2641
Preprint. Discussion started: 8 February 2024

mented within CHIMERE provided hourly concentrations of 6 chemical species including sulphates, nitrates, ammonium, primary and secondary organic particles, dust and BC. Aerosols were represented using a size bin approach with 10 bins with mean mass median diameters ranging from 10 nm to 40 m. Detailed information on the gas phase chemistry and secondary organic aerosol formation scheme used in this study (which is not directly relevant to the ultimate purpose of the current research) can be found in Veratti et al. (2023). In our investigation, we focused only on BC, which was treated as an inert species. Other parameterisations include the van Leer scheme (Van Leer, 1977) scheme for horizontal transport and the Troen and Mart formulation (Troen and Mahrt, 1986) for vertical turbulent mixing. In addition, wet and dry deposition processes of aerosols were considered using the equations of Henzing et al. (2006) and Zhang et al. (2001), respectively.

Boundary conditions were obtained from the national model kAIROS (AIR Operational System), which is the air quality forecast model operated by the regional air quality agency Arpae on a daily basis throughout Italy (Stortini et al., 2020), using the same version of CHIMERE used in this study with a spatial horizontal resolution of 7 km. The simulation period chosen for our study was from 4 February to 7 March 2020 and from 26 December 2020 to 21 January 2021, corresponding to the availability of BC measurements in Modena. In order to ensure the reliability and accuracy of our simulations, we implemented a spin-up period of 3 days in order to reach an equilibrium state and to establish stable initial conditions before the periods of interest.

In order to perform a source-tagged BC simulation aimed at distinguishing the contribution to total BC concentrations from different sources, we made modifications to the original CHIMERE code. These modifications allowed the specific allocation of the contribution of different sectors coming from outside the urban area of Modena.

2.4 GRAMM-GRAL description and set-up

The GRAMM-GRAL modelling system is a comprehensive approach designed for simulating air pollution in urban areas. It integrates two tools: GRAMM (Graz Mesoscale Model) and GRAL (Graz Lagrangian Model). While GRAMM focuses on the simulation of meteorological variables such as temperature, humidity, wind speed, and wind direction, GRAL is a Lagrangian particle dispersion model capable of reproducing pollutant concentrations in the atmosphere. This system is particularly well suited for simulating air pollution in urban environments, even in the presence of steep topography.

GRAMM is a non-hydrostatic model that addresses the conservation equations for mass, enthalpy, momentum, and humidity. It takes into account the effects of topography and surface interactions, such as the exchange of heat, momentum, humidity, and radiation, across different land use categories. To handle turbulence, an algebraic turbulence model (Pandolfo, 1969) is used when Gradient Richardson Numbers exceed 0.3, while a k- approach is used for lower values. Standard vertical profiles of wind and temperature are used to initiate and drive GRAMM at its boundaries, depending on the synoptic scale forcing and stability class chosen as input. The initialization process follows the Pasquill-Gifford classification and a detailed theoretical formulation and a practical implementation can be found in the works of Almbauer et al. (1995); Oettl (2015b). The ability of GRAMM in reproducing meteorological conditions with different topographic settings and resolutions has been demonstrated in previous studies such as, Almbauer et al. (1995); Oettl (2015b); Thunis et al. (2003); Oettl (2021); Oettl and Reifeltshammer

https://doi.org/10.5194/egusphere-2023-2641
Preprint. Discussion started: 8 February 2024

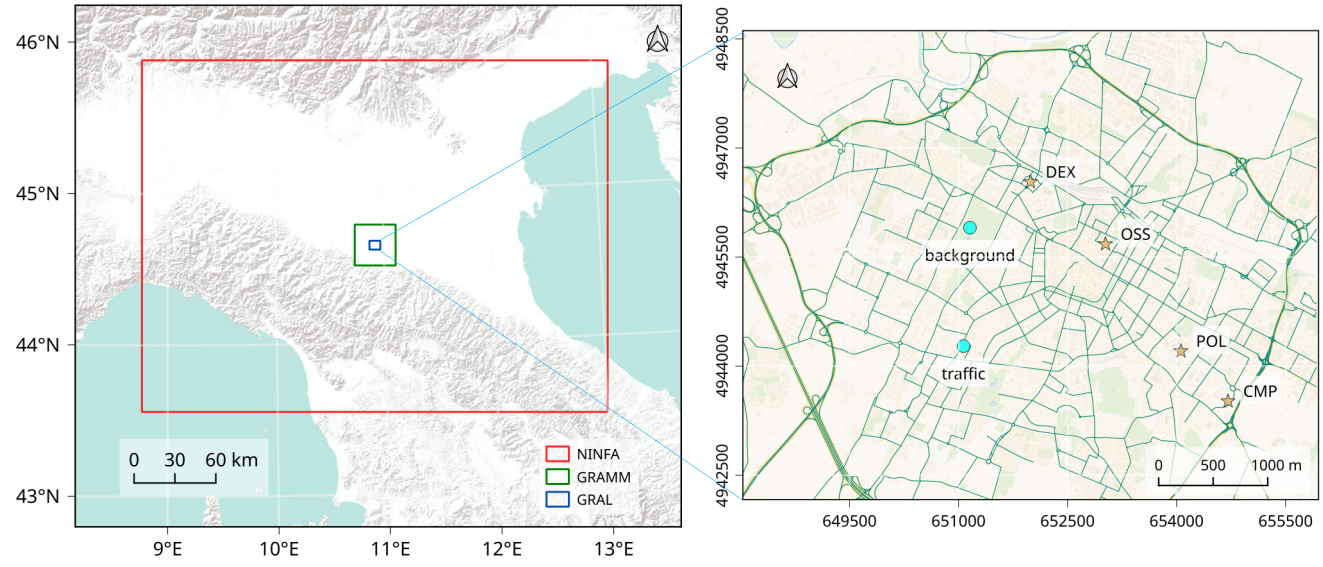

Figure 1. Spatial representation of the NINFA and GRAMM domains on the left, and the GRAL investigation domain on the right. The GRAL domain includes the positions of two urban air quality stations denoted by lightblue dots, specifically one located at the urban traffic (traffic) site and another at the urban background (background) site. Additionally, four meteorological stations used for meteorological validation and for selecting the meso-scale meteorological situation are indicated by yellow stars within the GRAL domain.

(2023). Furthermore, its performance has recently been evaluated by comparison with the widely used WRF model (Skamarock et al., 2008), showing very similar results for wind and temperature fields compared to observations (Oettl and Veratti, 2021).

Within GRAMM, the micro-scale model GRAL is embedded through a one-way coupling from the larger to the smaller scale. GRAL offers the option to operate in either diagnostic or prognostic mode. In the diagnostic mode, the flow field around buildings is determined by interpolating the large scale wind fields from GRAMM output assuming a logarithmic wind profile close to urban surfaces, then a Poisson equation is applied to correct velocities and guarantee the mass conservation. On the other hand, the prognostic mode, despite its higher computational cost, ensures superior accuracy by explicitly computing the flow through forward integration of the Reynolds-Averaged Navier-Stokes equations (RANS; Oettl (2015c)), while turbulence is estimated using a standard $k-\epsilon$ approach, neglecting Coriolis and buoyancy forces (Oettl, 2015c).

In this research, a cascade of scales was used to determine wind patterns within the city, from the synoptic to the building level. The study started with the simulation of large-scale meteorological conditions in the region surrounding the city of interest. An area of 30 km x 30 km was considered, centred on Modena, with a resolution of 200 m (see Figure 1). The simulation was carried out using GRAMM version 22.09, taking into account the local topography obtained from the Geoportale-Emilia-Romagna (2023) and land use data extracted from the Corine land cover database, updated to 2018 (CCL, 2018). These mesoscale flow patterns were used as the driving force for the computation of high-resolution winds within the city, specifically accounting for buildings and street canyons. Finally, Lagrangian dispersion calculations were performed using the dispersion

https://doi.org/10.5194/egusphere-2023-2641
Preprint. Discussion started: 8 February 2024

module of GRAL (version 22.09), with constraints imposed by the previously generated micro-scale wind fields. The GRAL domain includes the historical city centre, the ring road and most of the urban environment of Modena, covering a domain of approximately 7.9 km x 6.5 km, with a horizontal resolution of 4 m (see Figure 1).

Since the computation of the city-scale wind field at 4 m resolution over an entire urban environment is computationally intensive, the approach of Berchet et al. (2017) was implemented using a discrete representation of different weather situations. This approach took into account the classification of atmospheric stability, large-scale wind speed and direction at the boundaries of the domain into discrete categories. Large-scale wind directions were divided into 36 classes of 10 degrees each, while wind speeds were classified into 15 classes ranging from 0.25 to 7 $\mathrm{m\,s^{-1}}$. Atmospheric stability was classified according to the the Pasquill-Gifford classes (EPA, 2000). This resulted in a catalogue of about 1100 physically meaningful reference weather situations that occurred during the two periods of interest. Once the catalogue of meteorological situations was completed, at each simulation time step the wind field was selected by matching the meteorological catalogue with the observed meteorological conditions at the reference urban stations within the urban area of Modena (see Figure 1). Lagrangian dispersion calculations were then performed at hourly intervals in prognostic mode. In order to validate the model wind fields at the urban scale, we used the same stations that were used to select the wind field situation from the catalogue. The location of the stations is shown in Figure 1, while their characteristics are reported in Table 1. On the other hand, the validation of the results obtained with NINFA and GRAL was carried out using eBC measurements at two sites, respectively urban background and traffic sites.

2.5 Anthropogenic emissions

2.5.1 City scale

The anthropogenic emissions used in this study were obtained from the regional emission inventory for the Emilia-Romagna region, regularly compiled by the local environmental agency Arpae (INEMAR, 2023). This inventory provides annual totals of $\mathrm{PM_{10}}$, $\mathrm{PM_{2.5}}$, $\mathrm{NO_x}$, CO, $\mathrm{SO_2}$, $\mathrm{NH_3}$ and non-methane volatile organic compounds (NMVOCs) for each municipality, in this case specifically for the year 2017. For transport emissions, however, we used a bottom-up approach rather than relying solely on the regional inventory. The latter has been shown to be successful in reporting high-resolution traffic emissions in previous studies conducted in the same region (Ghermandi et al., 2019, 2020; Veratti et al., 2020, 2021).

To estimate traffic emissions at the city scale, we employed a comprehensive bottom-up approach that integrates emission factors (EF) and activity data. The activity data was derived from traffic flows simulated by the PTV VISUM model. Then, specific exhaust EF were applied to estimate the total emissions, taking into account various factors such as fleet composition, vehicle type, fuel, engine capacity, load displacement, road slope, Euro emission standard and average travelling speed. Additionally, we considered non-exhaust traffic EF, which are contingent upon vehicle weight and travelling speed, to estimate emissions from tire, brake and road wear.

To estimate BC exhaust emissions from road transport, we adopted the Tier 3 methodology outlined in the European EMEP/EEA guidelines (Ntziachristos and Samaras, 2019), which includes the calculation of both hot emissions, which occur

https://doi.org/10.5194/egusphere-2023-2641
Preprint. Discussion started: 8 February 2024

when the engine is operating at its normal temperature, and emissions during transient thermal engine operation, commonly referred to as 'cold start' emissions. To determine the EF for each vehicle fleet category, we used flow velocity estimates from PTV VISUM, and the individual EFs were averaged taking into account the local fleet composition (ACI, 2023) and the total annual kilometres travelled by each vehicle category considered (ISPRA, 2023). As a result, we obtained two EFs per road segment: one for light vehicles (such as cars and mopeds) and another for light and heavy commercial vehicles. This estimate corresponds to the two classes available in the PTV VISUM output and allows a consistent representation of BC exhaust emissions.

On the other hand, for the estimation of non-exhaust BC traffic emissions, the Tier 2 approach described in Ntziachristos and Boulter (2019) was implemented. The calculation was based on the so-called "detailed methodology", which takes into account the speed dependency of tyre and brake wear emissions from moving vehicles, while for road surface wear the emissions depend only on the number of vehicles travelling on a given road. The exhaust and non-exhaust calculation methods used in this study were coded in the R programming language and embedded in a package called VERT (Vehicular Emissions from Road Traffic). The VERT package provides a comprehensive framework for estimating emissions from road traffic, including exhaust, non-exhaust and evaporative emissions. The calculation process takes into account fleet composition and vehicle flows for cars, mopeds, light-duty vehicles and trucks or aggregated classes depending on the level of data available. This package includes not only the latest emission factors and methodologies recommended by the European EMEP/EEA guidelines for BC emissions, but also for a range of other pollutants including CO, NO, primary NO_2, NO_x, VOC, CH_4, PM, Organic Carbon, N_2O, NH_3, CO_2 and SO_2. Furthermore, in recognition of the significant uncertainties associated with PM speciation in the determination of BC emission factors, VERT provides an uncertainty range for both exhaust and non-exhaust emission determination based on the speciation interval specified in the methodology documentation (Ntziachristos and Samaras, 2019; Ntziachristos and Boulter, 2019). In this study, we aimed to assess the impact of emission uncertainties on the model results and investigate the potential range of outcomes. To achieve this, we ran a series of scenarios incorporating different hypotheses regarding BC speciation factors and the distribution of emission sources within the city boundaries. This approach allowed us to obtain a comprehensive set of BC concentration maps covering a plausible range of outcomes.

For traffic emissions, we ran a base case scenario using the reference speciation factor for BC as suggested by the European EMEP/EEA guidelines, and two additional scenarios using the lower and upper range values for BC speciation. In addition, to increase the comprehensiveness of our assessment of the overall impact of traffic, we extended the emission estimate beyond exhaust and non-exhaust BC emissions and added resuspension due to traffic circulation. To include this source, we conducted five additional scenarios. Fuor of these were derived from the methodology proposed by Amato et al. (2012) and implemented as described in the HERMESv3 model (Guevara et al., 2020), while the fifth was evaluated based on the formulation of the NORTRIP model by Denby et al. (2013). Amato's approach relies on vehicle-specific emission factors, the values of which used in this study are detailed in Table 2. On the other hand, the NORTRIP formulation is based on ensuring mass conservation on the road surface. For the latter reason, we used a three-step procedure to estimate the resuspension effects using the NORTRIP model. First, we calculated the dispersion of the full set of emissions, including traffic exhaust, non-exhaust and emissions from other activity sectors. Then we used the BC deposition on the road surface obtained from this calculation to estimate the

https://doi.org/10.5194/egusphere-2023-2641
Preprint. Discussion started: 8 February 2024

Table 2. Simulated emission scenarios for traffic sources.

Label	Scale	Type	Light duty vehicles	Commercial vehicles
TRF-exh-1	City	exhaust	average BC speciation factor[a]	average BC speciation factor[a]
TRF-exh-2	City	exhaust	minimum BC speciation factor[a]	minimum BC speciation factor[a]
TRF-exh-3	City	exhaust	maximum BC speciation factor[a]	maximum BC speciation factor[a]
TRF-nexh-1	City	non-exhaust	average BC speciation factor[b]	average BC speciation factor[b]
TRF-nexh-2	City	non-exhaust	minimum BC speciation factor[b]	minimum BC speciation factor[b]
TRF-nexh-3	City	non-exhaust	maximum BC speciation factor[b]	maximum BC speciation factor[b]
TRF-res-1	City	resuspension	1.2 mg vehicle^{-1}	2.5 mg vehicle^{-1}
TRF-res-2	City	resuspension	1.65 mg vehicle^{-1}	1.65 mg vehicle^{-1}
TRF-res-3	City	resuspension	0.6 mg vehicle^{-1}	0.6 mg vehicle^{-1}
TRF-res-4	City	resuspension	2.7 mg vehicle^{-1}	2.7 mg vehicle^{-1}
TRF-res-5	City	resuspension	NORTRIP model	NORTRIP model
TRF-bck-1	Regional	exhaust, non-exhaust and resuspension	average BC speciation factor[a,b]	average BC speciation factor[a,b]
TRF-bck-2	Regional	exhaust, non-exhaust and resuspension	minimum BC speciation factor[a,b]	minimum BC speciation factor[a,b]
TRF-bck-3	Regional	exhaust, non-exhaust and resuspension	maximum BC speciation factor[a,b]	maximum BC speciation factor[a,b]

[a] See table 3-91 of Ntziachristos and Samaras (2019) for the exhaust PM speciation factors for different vehicle technologies.
[b] See table 3-4 and table 3-6 of Ntziachristos and Boulter (2019) for non-exhaust emission factor range for different vehicle categories.

resuspension effects based on the formulation reported below (Eq. 3). Finally, we performed another simulation using these emission rates to determine the contribution of resuspension to atmospheric concentrations. The calculation of the resuspension rate Q_{resusp}, which represents the amount of particles resuspended into the atmosphere according to the NORTRIP model, is determined according to Eq. 4, taking into account the mass deposited on the road surface M_{dep}.

$$Q_{\text{resusp}} = M_{\text{dep}} \cdot F_{\text{resusp}} \tag{3}$$

Where F_{resusp} is the resuspesion factor and can be calculated as:

$$F_{\text{resusp}} = \sum_{v=1}^{2} N_{\text{v}} \left(\frac{u_{\text{v}}}{u_{\text{ref(r)}}} \right) f_{0,v} \tag{4}$$

The variables in the Eq. 4 are defined as follows: v represents the vehicle type, N_{v} represents the vehicle flow (measured in vehicles per hour), u_{v} represents the vehicle speed (measured in $\mathrm{km\,h^{-1}}$), $u_{\text{ref(r)}}$ represents the reference vehicle speed for the resuspension process (measured in $\mathrm{km\,h^{-1}}$), and $f_{0,\text{v}}$ represents the reference mass fraction of the resuspension process per vehicle. In line with previous studies by Thouron et al. (2018); Denby et al. (2013); Lugon et al. (2021), this study adopts the values $u_{\text{ref(r)}} = 50\ \mathrm{km\,h^{-1}}$, $f_{0,\text{HDV}} = 5 \cdot 10^{-5}$ per vehicle, and $f_{0,\text{LDV}} = 5 \cdot 10^{-6}$ per vehicle. All traffic scenarios simulated in this study are summarised in Table 2.

A combination of speciation factors and detailed inventory data was used to estimate emissions from other activity sectors. As introduced at the beginning of this section, the Arpae inventory is used as a reference, while activity-dependent BC speciation factors reported by the EEA (2019) and listed in Table S2 in the Supplement were used to convert total PM emissions into

https://doi.org/10.5194/egusphere-2023-2641
Preprint. Discussion started: 8 February 2024

Table 3. Simulated emission scenarios for non-industrial combustion sources.

Label	Scale	Emissions assigned to rural areas (%)	Emissions assigned to discontinuous urban fabric (%)	Emissions assigned to the historical city centre (%)
DMH-1	City	80	20	0
DMH-2	City	60	40	0
DMH-3	City	50	50	0
DMH-4	City	50	40	10
DMH-5	City	40	40	20
DMH-bck-1	Regional	60	40	included in discontinuous urban fabric
DMH-bck-2	Regional	40	60	included in discontinuous urban fabric
DMH-bck-3	Regional	80	20	included in discontinuous urban fabric

BC estimates. In order to distribute the emissions within the urban area of Modena, land use data and building characteristics were used as proxy variables. However, it should be noted that in the Emilia-Romagna region there are still significant uncertainties regarding the distribution of emissions from biomass burning for non-industrial combustion. To address this limitation, we developed five different emission scenarios to capture the variability of emissions in terms of spatial distribution. These scenarios considered different source locations and different total emissions allocated to different areas of the city, including the historic centre, discontinuous urban fabric and rural areas. Table 3 summarises the characteristics of each scenario.

The daily temporal modulation of non-industrial combustion emissions is based on the concept of heating degree days, a metric developed to capture the energy demand required to heat a structure based on both external and internal temperatures. The formula used in this study to incorporate this calculation is derived from Mues et al. (2014). In addition to transport and biomass combustion, other relevant SNAP sectors included in the calculation are emissions from industry and other mobile machinery. However, due to their relatively small contribution in annual totals compared to transport and biomass burning, no additional scenarios were simulated to assess their impact range.

2.5.2 Regional scale

The emission data used for NINFA were taken from the same inventory used at the urban scale, where the total annual emissions for each pollutant are reported at the municipal level. This inventory presents the total annual emissions for each pollutant at the municipal level. To guarantee a precise depiction at a more detailed resolution, a downscaling procedure was implemented. This procedure involved scaling each SNAP category, taking into account monthly, daily, and hourly variations, with reference to a typical profile for northern Italy as described by Veratti et al. (2023). To avoid double counting of BC emissions within the urban area of Modena, the emission fluxes from this area were set to zero.

To assess the influence of external areas on BC concentrations in Modena, six scenarios were developed. Three scenarios focused on the speciation factors of both exhaust and non-exhaust traffic emissions. In particular, to convert the total PM emissions reported in the inventory into BC emissions, vehicle fleet dependent BC speciation factors calculated with the VERT

https://doi.org/10.5194/egusphere-2023-2641
Preprint. Discussion started: 8 February 2024

package were used. The first scenario used average BC conversion factors, while the other two scenarios represented the lower and upper bounds of the BC speciation values. For non-industrial combustion BC emissions, three different spatial allocations were considered. In the first allocation, municipal totals were distributed with 40% allocated to rural areas and 60% to urban areas. In the second allocation, the same proportion was maintained, but 60% was allocated to rural areas and 40% to urban areas. In the third allocation, 80% was allocated to rural areas and 20% to urban areas. Table 3 provides an overview of each scenario simulated at the regional level.

3 Model evaluation

A number of statistical metrics have been used to evaluate the hybrid modelling system against observed data. These metrics include Mean Bias (MB), Normalised Mean Bias (NMB), Pearson's correlation coefficient (r), the proportion of predicted values within a factor of two of the observations called Factor of Two (FAC2), Normalised Mean Square Error (NMSE), Fractional Bias (FB), Normalised Average Difference (NAD) and Root Mean Square Error (RMSE). Detailed definitions of these metrics can be found in Section S4 of the Supplementary material.

4 Results

4.1 Measurements from MA200

Figure 2 shows the average diurnal variability of the aerosol absorption at 880 nm (panel a) from the two MA200 instruments partitioned using the results of the MWAA model, distinguishing between fossil fuels, biomass combustion and BrC. The same partitioning was also used to differentiate eBC concentrations (panel b of Figure 2) between fossil fuels (eBC-FF) and biomass combustion (eBC-BB), applying a fixed MAE (see Section 2.1). Due to the lack of in situ validation measurements to assess the MAE of BrC and the significant uncertainty associated with its determination - see for example the diverse structures and properties of the wide range of chemical organic compounds, coupled with its sensitivity to variations in time and location - we chose not to convert b_{abs}^{BrC} into concentrations. This decision was taken to avoid introducing additional uncertainty associated with assuming a specific MAE for BrC.

The measurements reported in Figure 2 were carried out during two different periods. The first period lasted from 4 February to 7 March 2020, while the second period spanned from 26 December 2020 to 21 January 2021 for the traffic site and from 26 December 2020 to 7 January 2021 for the urban background.

When analysing the results, it can be seen that b_{abs}^{BrC} remain consistently very low on average throughout the day for both sites, averaging around 0.5 Mm^{-1} for the first period and around 1.2 Mm^{-1} for the second period. On the other hand, $b_{abs,BC}^{FF}$ shows the characteristic behaviour associated with traffic emissions, with two peaks during rush hours. Specifically, these peaks occur in the morning between 07:00 and 08:00 GMT and in the evening between 18:00 and 19:00 GMT or slightly delayed at the urban background site for the first period, between 18:00 and 20:00 GMT. This pattern is also observed for other traffic-

https://doi.org/10.5194/egusphere-2023-2641
Preprint. Discussion started: 8 February 2024

related tracers such as NO, NO_2 and benzene measured at the same two sites, not shown here but reported in a companion study by Bigi et al. (2023).

In contrast, $b_{abs,BC}^{BB}$ shows less variability and generally lower diurnal concentrations compared to $b_{abs,BC}^{FF}$. In particular, their behaviour is different, with $b_{abs,BC}^{BB}$ reaching a minimum in the early afternoon, typically between 15:00 and 17:00 GMT. This phenomenon can be attributed to a combination of factors, including a higher mixing layer depth and lower emissions during these hours. In the later part of the afternoon, after 17:00 GMT, $b_{abs,BC}^{BB}$ typically increase and reach a maximum between 20:00 and 21:00 GMT, when the emitting sources are likely to be at their peak emission levels and the mixing layer depth is gradually decreasing due to surface cooling. Despite a likely decrease in the intensity of biomass burning emissions during the night, $b_{abs,BC}^{BB}$ remain relatively high due to a temperature inversion that often characterises the area, while during the rest of the day $b_{abs,BC}^{BB}$ concentrations gradually decrease until reaching the minimum explained above.

Comparing the first and second periods, it is interesting to note that the mean absorption coefficient for BC of the second period was significantly higher than that of the first, with mean values for $b_{abs,BC}^{FF}$ (eBC-FF) and $b_{abs,BC}^{BB}$ (eBC-BB) of 19.7 ± 15.1 $\mathrm{Mm^{-1}}$ (1.94 ± 1.49 $\mu g\,m^{-3}$) and 4.5 ± 5.9 $\mathrm{Mm^{-1}}$ (0.44 ± 0.58 $\mu g\,m^{-3}$), respectively, at the traffic site for the first period and 29.4 ± 24.6 $\mathrm{Mm^{-1}}$ (2.90 ± 2.43 $\mu g\,m^{-3}$) and 13.3 ± 11.2 $\mathrm{Mm^{-1}}$ (1.32 ± 1.11 $\mu g\,m^{-3}$) for the second period at the same station. $b_{abs,BC}^{BB}$ (eBC-BB) at the urban background site expresses the similar behaviour with a mean value equal to 5.2 ± 4.7 $\mathrm{Mm^{-1}}$ (0.52 ± 0.46 $\mu g\,m^{-3}$) for the first period and to 9.6 ± 8.7 $\mathrm{Mm^{-1}}$ (0.95 ± 0.86 $\mu g\,m^{-3}$) for the second period. A possible explanation for this increase can be found in the different meteorological conditions in the two periods. More specifically, as described in Section S6 of the Supplement, the second period shows more stagnant conditions compared to the first period. This is due to more stable atmospheric conditions, characterised by recurrent thermal inversions (Figures S7 and S8) and a higher frequency of stable atmospheric classes compared to the first period (Figures S2 and S3) which have likely led to lower mixing layer height. The frequency of occurrence of stable atmospheric classes (G and F, according to the Pasquill and Guilford formulation) is 0.53 for the first period and 0.63 for the second period. In addition, the mean hourly temperature observed at the OSS station, representing the urban area, was significantly lower in the second period (2.9 °C) compared to the first period (9.4 °C). This probably led to an increase in biomass burning for domestic heating, contributing significantly to the total eBC concentrations (see Figures 2).

On the other hand, $b_{abs,BC}^{FF}$ (eBC-FF) at the urban background site shows a different trend. Contrary to the other site and $b_{abs,BC}^{BB}$, its mean value decreased from 9.8 ± 7.1 $\mathrm{Mm^{-1}}$ (0.97 ± 0.70 $\mu g\,m^{-3}$) in the first period to 7.3 ± 5.5 $\mathrm{Mm^{-1}}$ (0.72 ± 0.55 $\mu g\,m^{-3}$) in the second period. The most plausible explanation for this discrepancy lies in the type of days included in the second period. Specifically, the measurements at the urban background site were taken over a period of 13 days, 7 of which coincided with holidays during the Christmas time, resulting in lower traffic volumes throughout the city. It is therefore reasonable to expect a limited contribution from traffic during this period. Furthermore, it is worth noting the impact of strong stagnation conditions that occurred in Modena between 13-14 and 18-19 January 2021 (see Figure S2 and Figure 5), verified after the end of the measurements at the urban background site.

https://doi.org/10.5194/egusphere-2023-2641
Preprint. Discussion started: 8 February 2024

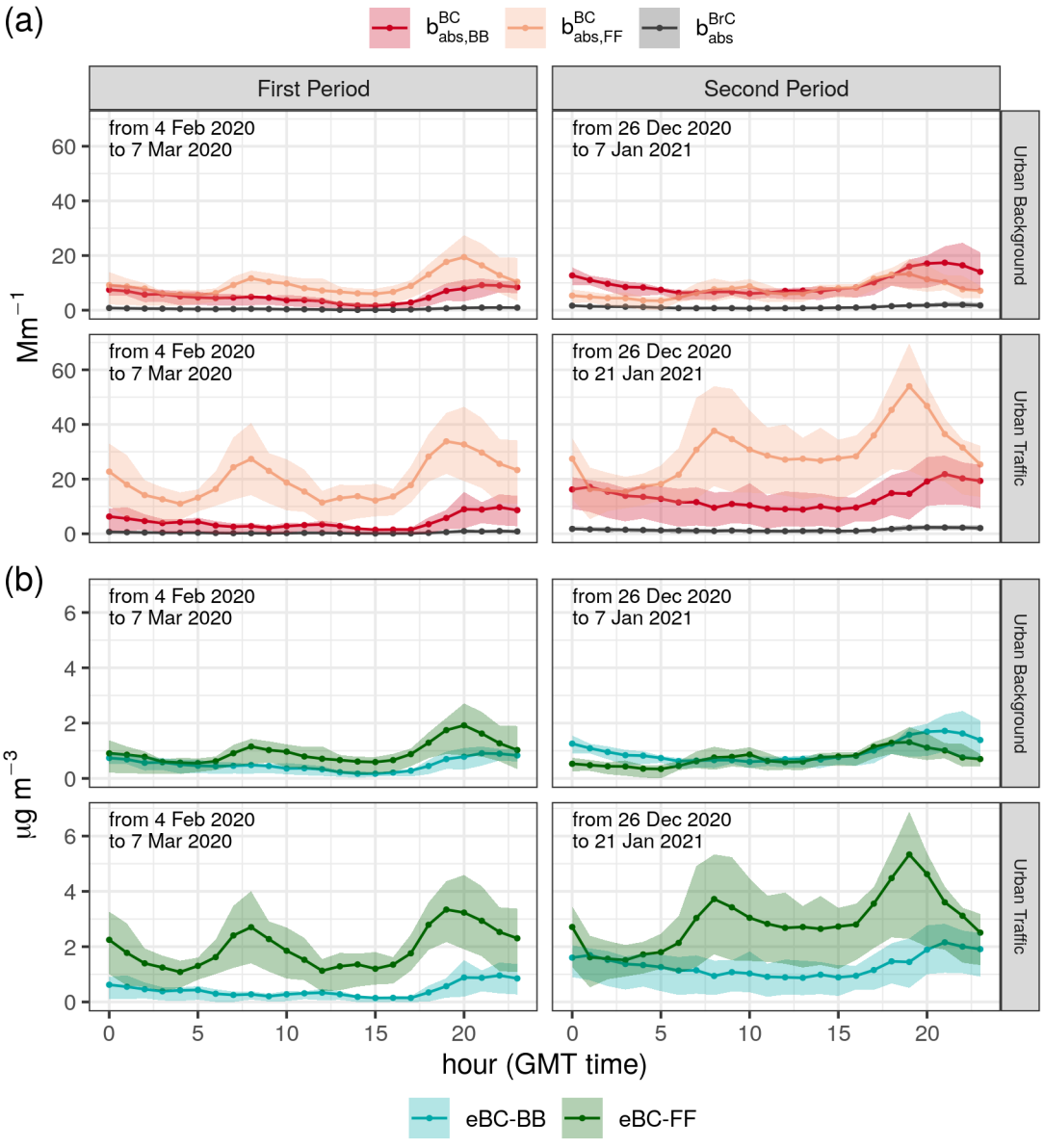

Figure 2. Average daily cycle of $b_{abs,BC}^{BB}$, $b_{abs,BC}^{FF}$, and b_{abs}^{BrC} is shown for panel (a), while panel (b) displays eBC-BB and eBC–FF concentrations, all apportioned using the MWAA model. The solid lines represent the average absorptions or concentrations, while the shaded areas indicate the interquartile range. The top panels illustrate concentrations measured at the urban background site, while the bottom panels display concentrations measured at the traffic site.

https://doi.org/10.5194/egusphere-2023-2641
Preprint. Discussion started: 8 February 2024

Table 4 shows the average results of the MWAA model, providing insight into the partitioning of components (BC vs. BrC) and sources (FF vs. BB) for both the first and second periods of our investigation. Furthermore, the table shows the results of the MWAA and Aethalometer model partitioning, as well as the results of the application of the EPA PMF 5.0, using hourly absorption data and elemental concentrations, as observed in previous research carried out in the Po Valley. The comparative analysis underlines the consistency of the results obtained in our study using MA200 instruments, which are on average in line with the findings of other studies carried out in the same region.

https://doi.org/10.5194/egusphere-2023-2641
Preprint. Discussion started: 8 February 2024

Table 4. Summary table of component (BC vs. BrC) and source (FF vs. BB) apportionment based on this work and other literature studies conducted in the Po valley. Most values are reported at 880 nm, with the exception of Forello et al. (2019), which present data at 780 nm. RB, UB, and UT stand for Rural Background, Urban Background and Urban Traffic respectively.

City	Site type	Period	Instrument	BC-FF (%)	BC-BB (%)	BrC (%)	Reference
Milan	UB	Jan-Feb 2018	AE33[a,1]	68	32	-	Bernardoni et al. (2021)
Milan	UB	Jan-Feb 2018	AE31[a,1]	68	32	-	
Milan	UB	Jan-Feb 2018	AE33[b,1]	72	28	-	
Milan	UB	Jan-Feb 2018	AE31[b,1]	77	23	-	
Milan	UB	Jan-Feb 2018	in-house polar photometer[1]	76	24	-	
Milan	UB	Jan-Feb 2018	AE33[a,2]	94*		6	
Milan	UB	Jan-Feb 2018	AE31[a,2]	91*		9	
Milan	UB	Jan-Feb 2018	AE33[c,2]	91*		9	
Milan	UB	Jan-Feb 2018	AE31[c,2]	95*		5	
Milan	UB	Jan-Mar 2018	AE31 and AE51[1]	39	61	-	Mousavi et al. (2019)
Bareggio	RB	Jan-Mar 2018	AE31 and AE51[1]	64	36	-	
Milan	UB	21-28 Nov 2016	in-house polar photometer[d]	55	20	-	Forello et al. (2019)
Milan	UB	Nov 2015-Jan 2016	AE31[1]	63	37	-	Ferrero et al. (2018)
Modena	UT	Feb-Mar 2020	MA200[2]	80	18	2	This study
Modena	UB	Feb-Mar 2020	MA200[2]	63	34	3	
Modena	UT	Dec 2020-Jan 2021	MA200[2]	67	31	2	
Modena	UB	Dec 2020-Jan 2021	MA200[2]	40	54	6	

[a] seven wavelength (370, 470, 520, 590, 660, 880 and 950 nm) fit with fixed multiple-scattering enhancement parameter.

[b] four wavelength (470, 520, 660 and 880 nm) fit with fixed multiple-scattering enhancement parameter.

[c] five wavelength (470, 520, 590, 660 and 880 nm) fit with fixed multiple-scattering enhancement parameter.

[d] Source apportionment was conducted using EPA PMF 5.0, incorporating hourly absorption data at four distinct wavelengths (405, 532, 635 780 nm), in combination with hourly elemental concentrations from samples gathered and analysed on the same filters. The outcomes of this analysis revealed that the third factor in the apportionment could be attributed to sulphate, constituting approximately 20% of the overall composition. The fourth factor, on the other hand, was primarily composed of resuspended dust, accounting for approximately 4% of the total, with other factors of lesser significance contributing approximately 1%.

[1] Aethalomter model.

[2] MWAA model.

* Total BC, represents the cumulative sum of BC-FF and BC-BB.

https://doi.org/10.5194/egusphere-2023-2641
Preprint. Discussion started: 8 February 2024

4.2 Modelling results

4.2.1 Meteorology

Using the GRAMM-GRAL modelling system, a comprehensive catalogue of meso- and micro-scale flow patterns was calculated. Following the methodology outlined in Section 2.4, a series of hourly wind fields were generated to drive the Lagrangian dispersion in Modena. Whenever possible, meteorological observations from the stations shown in Figure 1 were used. First, the wind fields were computed independently of any observation, following the discretisation procedure described in Section 2.4. Subsequently, the wind fields were selected to closely match the actual conditions. It is important to acknowledge that although a given wind field from the catalogue may not be perfectly consistent with all stations simultaneously, this study relies exclusively on data from stations located in the urban area of Modena to construct the catalogue. This is due to the unavailability of measurements from other locations within the GRAMM domain and within a range of 50-60 km. Furthermore, considering that the area of interest is almost flat, we expect that this setup will not significantly affect the representation of the flow fields in the area of interest. Figure 3 shows the comparison between modelled and measured hourly wind speed for the available urban stations for the period of interest. Panel (a) represents the first period, while panel (b) shows the wind speed comparison for the second period. Despite some notable underestimations of the observed wind speed on 5, 10, 26, 27 and 28 February 2020, due to the wind category discretisation process, GRAMM-GRAL generally reproduced the trend quite well for both periods. For the first period the wind speed is generally underestimated, with MB between -0.44 $\mathrm{m\,s^{-1}}$ and -0.27 $\mathrm{m\,s^{-1}}$ at CMP and OSS respectively (corresponding to -34% and -9% of the NMB), while at DEX the NMB is approximately zero and the MB is 0.02 $\mathrm{m\,s^{-1}}$. Similarly, during the second period, the wind speed is generally underestimated at CMP and POL, with MB values of -0.28 $\mathrm{m\,s^{-1}}$ and -0.03 $\mathrm{m\,s^{-1}}$, respectively, while it is overestimated at OSS with an MB of 0.31 $\mathrm{m\,s^{-1}}$. The corresponding NMB values are -37%, -2%, and +20%, respectively. The RMSE of the simulated wind speed by GRAMM-GRAL is 0.88 $\mathrm{m\,s^{-1}}$, 0.72 $\mathrm{m\,s^{-1}}$ and 1.16 $\mathrm{m\,s^{-1}}$ for CMP, OSS, and DEX during the first period, and 0.60 $\mathrm{m\,s^{-1}}$, 0.83 $\mathrm{m\,s^{-1}}$ and 0.89 $\mathrm{m\,s^{-1}}$ for CMP, POL, and OSS during the second period. These RMSE values are in line with the recommended statistical benchmark suggested by the EEA guidelines for meteorological wind field assessment (EEA, 2011), which suggests RMSE values of less than 2 $\mathrm{m\,s^{-1}}$. Other statistical indices, including FAC2, NMSE and r, are reported in Table 5 and the related scores are consistent with similar studies conducted in the same area during previous simulation years (Veratti et al., 2020, 2021). To complement the wind speed analysis, Figure S4 displays wind roses comparing the modelled and observed wind speed and direction for the same stations discussed above. The wind roses confirm that the modelling system effectively reproduces many of the observed features, with the observed winds being generally well captured by GRAMM-GRAL, especially during the second period.

https://doi.org/10.5194/egusphere-2023-2641
Preprint. Discussion started: 8 February 2024

Table 5. Statistical analysis of hourly wind speed computed at urban meteorological stations using the GRAMM-GRAL modelling system.

Station	Period	MB ($m\,s^{-1}$)	NMB (%)	RMSE ($m\,s^{-1}$)	NMSE	FAC2	r
CMP	first period	-0.44	34	0.88	0.27	0.67	0.71
DEX	first period	0.02	0	1.16	0.72	0.73	0.77
OSS	first period	-0.27	9	0.72	0.07	0.97	0.95
CMP	second period	-0.28	37	0.60	0.98	0.42	0.55
OSS	second period	0.31	20	0.83	0.23	0.76	0.75
POL	second period	-0.03	2	0.89	0.23	0.72	0.61

https://doi.org/10.5194/egusphere-2023-2641
Preprint. Discussion started: 8 February 2024

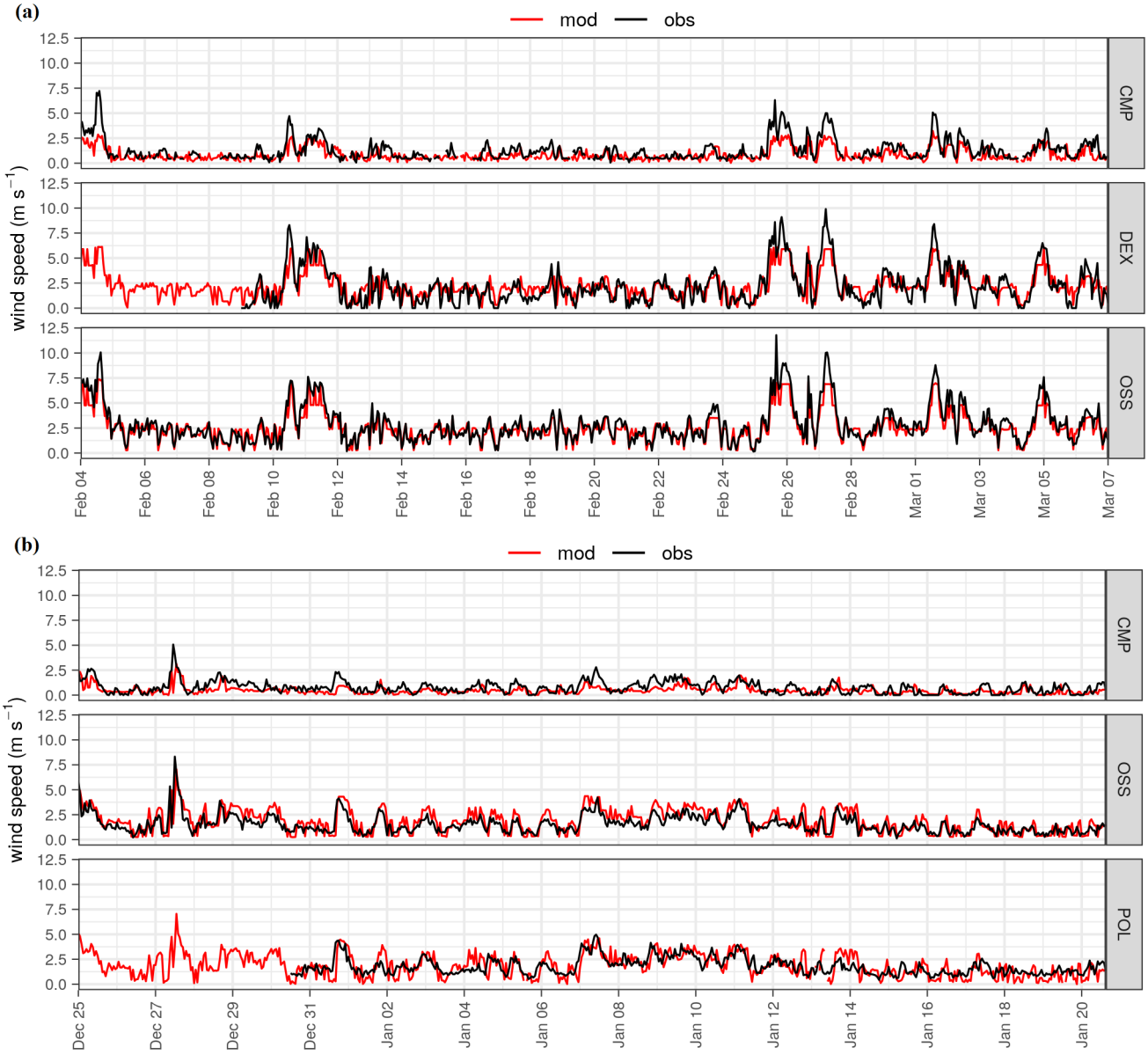

Figure 3. Hourly time series of measured wind speed (black) at four urban meteorological stations in Modena, alongside micro-scale modelled values by GRAMM-GRAL (red) for two periods: (a) 4 February to 7 March 2020, and (b) 26 December 2020 to 21 January 2021.

https://doi.org/10.5194/egusphere-2023-2641
Preprint. Discussion started: 8 February 2024

4.2.2 Comparative analysis of modelled BC concentrations using a hybrid Eulerian-Lagrangian modelling system in Modena

The background BC concentrations derived from NINFA in the urban area of Modena were integrated with the BC concentrations simulated by the GRAMM-GRAL modelling system, which specifically considers emissions only at the urban scale. The scenarios considered for the evaluation include TRF-exh-1 for traffic exhaust emissions and TRF-nexh-1 for non-exhaust emissions. In the case of resuspension and biomass burning, which are characterised by a high level of uncertainty, the average concentrations calculated from all simulated scenarios were taken into account. For NINFA, the scenarios TRF-bck-1 and DMH-bck-1 were considered. This specific emission configuration will be referred to as the base case scenario.

To evaluate the effectiveness of the hybrid modelling system in various urban settings, modelled concentrations at station locations were compared with observed eBC levels from MA200 devices. Figures 4 and 5 show the time series comparing measured (eBC) and modelled (BC) concentrations, divided into their contributors (biomass burning, fossil fuels and non-exhaust+resuspension) for the first and second periods, respectively. The analysis reveals a notably robust performance of the hybrid system in modelling concentrations during the first simulated period (5 February - 8 March, 2020). The bias is very low at both sites: MB is -0.12 $\mu g\,m^{-3}$ for urban traffic (corresponding to -5% of NMB) and 0.03 $\mu g\,m^{-3}$ for urban background (corresponding to +2%). The Pearson correlation coefficient between modelled and observed concentrations is 0.62 at the traffic site and 0.51 at the urban background station. In addition, the modelling system generally captured the daily peaks correctly, even under different meteorological conditions. In particular, several relatively high wind speed episodes for typical Modena meteorological conditions occurred during this period, such as on 5, 11, 12, 26, 28 February, and 2, 5 March 2020, with speeds reaching 11.2 $m\,s^{-1}$. The modelling system showed adaptability in simulating both calm and windy periods. Conversely, the performance of the model in reproducing observations decreased during the second period (26 December 2020 - 21 January 2021), as observed eBC concentrations experienced significantly higher values than in the first period. The Pearson correlation coefficients between modelled and observed concentrations are 0.34 and 0.38 at the traffic and background sites, respectively. The corresponding MB are -0.92 $\mu g\,m^{-3}$ (corresponding to -22% of NMB) and +0.25 $\mu g\,m^{-3}$ (corresponding to +15% of NMB) at the same two stations. Favourable meteorological conditions for the accumulation of pollutants were observed both in Modena and in the surrounding areas. These conditions were mainly characterised by high pressure systems and persistent thermal inversions in the lower atmospheric layers, resulting in a likely shallow mixing layer height. This meteorological pattern, combined with the probable presence of sporadic high emitting sources in the vicinity of the measurement site (see section S6 in the Supplement for further explanations), contributed to the elevated eBC concentrations observed, up to 18 $\mu g\,m^{-3}$ at the urban traffic site (Figure 5). Under these exceptional circumstances, the Hybrid system had difficulties in reproducing the observed concentration pattern.

Despite the decrease in the performance of the hybrid modelling system compared to the first period, the metrics of FB, NMSE, FAC2 and NAD closely match with the results reported by Lugon et al. (2021) when simulating BC concentrations in a suburban street network of Paris using the Street-in-Grid model. Furthermore, the corresponding metrics of FB, NMSE, FAC2 and NAD in this study for both periods, reported in Table 6 together with the previously mentioned indices, largely meet the

https://doi.org/10.5194/egusphere-2023-2641
Preprint. Discussion started: 8 February 2024

Table 6. Statistical analysis of hourly total BC concentrations at urban traffic and urban background sites using the hybrid modelling system.

Station	Period	MB ($\mu g\,m^{-3}$)	NMB (%)	RMSE ($\mu g\,m^{-3}$)	NMSE	FAC2	r	FB	NAD
Urban Traffic	first period	-0.12	-5	1.38	0.34	0.80	0.62	0.05	0.02
Urban background	first period	0.03	2	1.02	0.34	0.67	0.51	0.05	0.02
Urban Traffic	second period	-0.92	-22	2.89	0.60	0.69	0.34	0.25	0.13
Urban background	second period	0.25	15	1.13	0.35	0.72	0.38	-0.13	0.06

acceptance criteria established by Hanna and Chang (2012) for urban dispersion modelling, where the benchmark values are defined as follows:

- FAC2 > 0.30
- NAD < 0.50
- |FB| < 0.67
- NMSE < 6

https://doi.org/10.5194/egusphere-2023-2641
Preprint. Discussion started: 8 February 2024

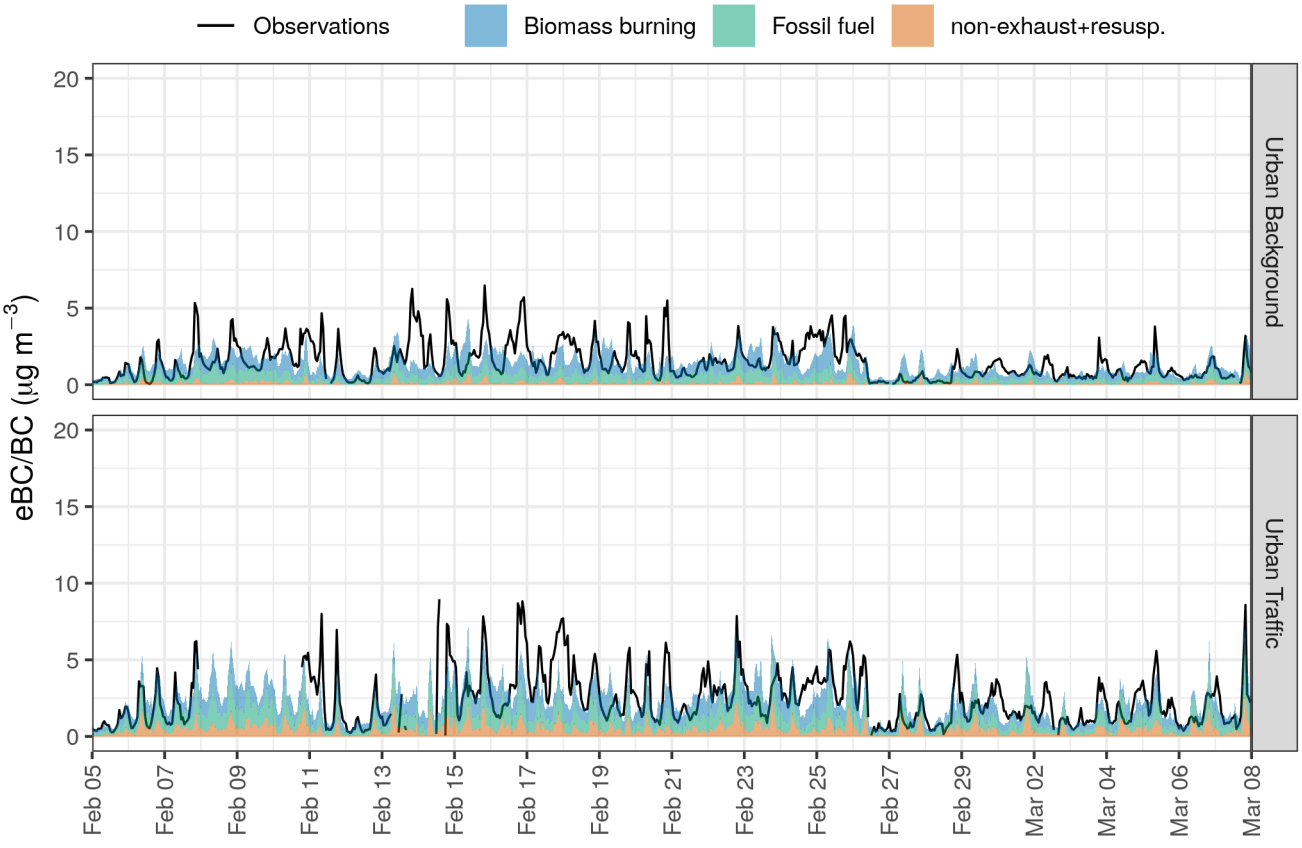

Figure 4. Hourly time series of observed (eBC) and simulated (BC) concentrations at urban traffic and background site for the first period (from 4 February to 7 March 2020). Simulated concentrations are separated by contributions from the main emission categories (biomass burning, fossil fuel and non-exhaust+resuspension).

https://doi.org/10.5194/egusphere-2023-2641
Preprint. Discussion started: 8 February 2024

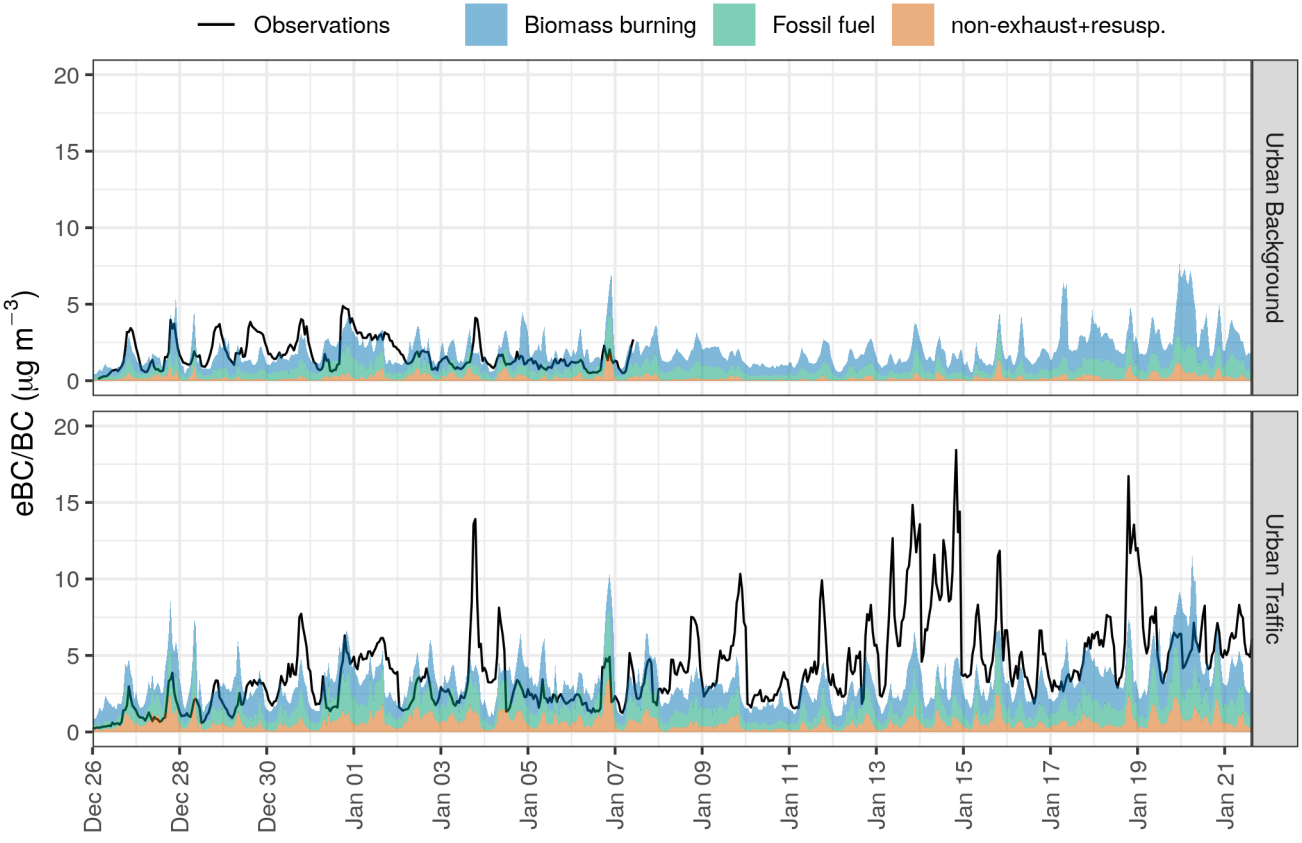

Figure 5. Hourly time series of observed (eBC) and simulated (BC) concentrations at urban traffic and background site for the second period (from 26 December 2020 to 21 January 2021). Simulated concentrations are separated by contributions from the main emission categories (biomass burning, fossil fuel and non-exhaust+resuspension).

https://doi.org/10.5194/egusphere-2023-2641
Preprint. Discussion started: 8 February 2024

The MWAA model, applied to MA200 measurements with additional hypotheses about α for different sources, enabled to dishern the contributions of different sectors to observed eBC concentrations (see Section 2.1). This approach allowed for the assessment of the hybrid system's performance in reproducing concentrations of two distinct sources: fossil fuel and biomass burning. Figures 6 and 7 present the diurnal patterns of observed and modelled concentrations, respectively for the first and second simulated periods, for total BC (eBC/BC, panel a), BC from fossil fuel (eBC-FF/BC-FF, panel b), and BC from biomass burning (eBC-BB/BC-BB, panel c). In addition, in order to assess the influence of emission uncertainties on the model outputs and explore potential outcome ranges, the figures for BC-FF and BC-BB also include the uncertainty range resulting from the emission scenarios described in Section 2.5. Error bars indicate the minimum and maximum average concentrations derived from different scenarios. The points correspond to the average concentrations of the base case scenario. Additionally, to provide additional details, blue shaded areas depict the interquartile range derived from the base case scenario, while red shaded areas represent the interquartile range of observed concentrations.

Due to a limitation in the MWAA model, it is not possible to separate the influence of non-exhaust and resuspension from the total eBC concentrations without additional experimental data. Therefore, where not explicitly stated, the modelled BC-FF concentrations in this section include the combined contribution of fossil fuels, traffic non-exhaust and traffic resuspension.

During the first period (as shown in Figure 6, panel a), it is noteworthy that despite a slight underestimation of the measured concentrations occurring between 03:00 and 06:00 GMT and a slight overestimation observed between 18:00 and 21:00 GMT both at the urban background site, the simulation shows a good agreement with measurements at both locations. Looking at the specifics of the eBC-FF/BC-FF concentrations (Figure 6, panel b), the base case scenario proves to be generally effective in representing the average trends, despite a slight underestimation between 18:00 and 21:00 GMT at both sites during the second peak of daily rush hours. This discrepancy could probably be attributed to an inherent underestimation of traffic flows during this specific time period, a trend that is consistent with the results of the second period and with the findings of Veratti et al. (2021), who performed a comprehensive analysis of the same area with respect to nitrogen oxides concentrations. Nevertheless, the overall agreement of model results with observations further confirms the effectiveness of a bottom-up approach in accurately representing traffic emissions.

Focusing on the contribution of biomass burning to total BC (Figure 6, panel c), it is interesting to note that during the first half of the day, particularly between 03:00 and 11:00 GMT, the observations are close to the lower bound indicated by the error bars. This suggests that the collective average of all scenarios tends to slightly overestimate the observed trend during this period. Conversely, the experimental eBC-BB pattern could also be underestimated, possibly due to measurement uncertainties associated with the MA200 instruments, as reported in recent studies (Alas et al., 2020; Li et al., 2021). More specifically, the observations between 03:00 and 11:00 GMT show a stronger agreement with the results generated by the DMH-2 scenario at the urban background location and by the DMH-4 scenario at the urban traffic location. Conversely, the peak in eBC-BB concentrations occurring after 19:00 GMT is remarkably well represented by the average concentration derived from all modelled scenarios. These results lead to two plausible interpretations. The first suggests that the hourly modulation profile used to distribute the emissions over the day takes into account a morning peak that may not be prevalent on average among the sources within Modena (see Figure S10 in the Supplement for the emission daily modulation profile used in this study).

https://doi.org/10.5194/egusphere-2023-2641
Preprint. Discussion started: 8 February 2024

The same hypothesis suggests that the distribution of emissions among the different districts of the city could possibly be an intermediate situation between those presented in this study (i.e. DMH-1, DMH-2, DMH-3, DMH-4 and DMH-5 scenarios). The second alternative explanation suggests that the emission allocation is a mixture of those represented by scenarios DMH-2 and DMH-4 and that the hourly modulation profile underestimates the emission peak during the night hours when the observations express the highest concentrations.

https://doi.org/10.5194/egusphere-2023-2641
Preprint. Discussion started: 8 February 2024

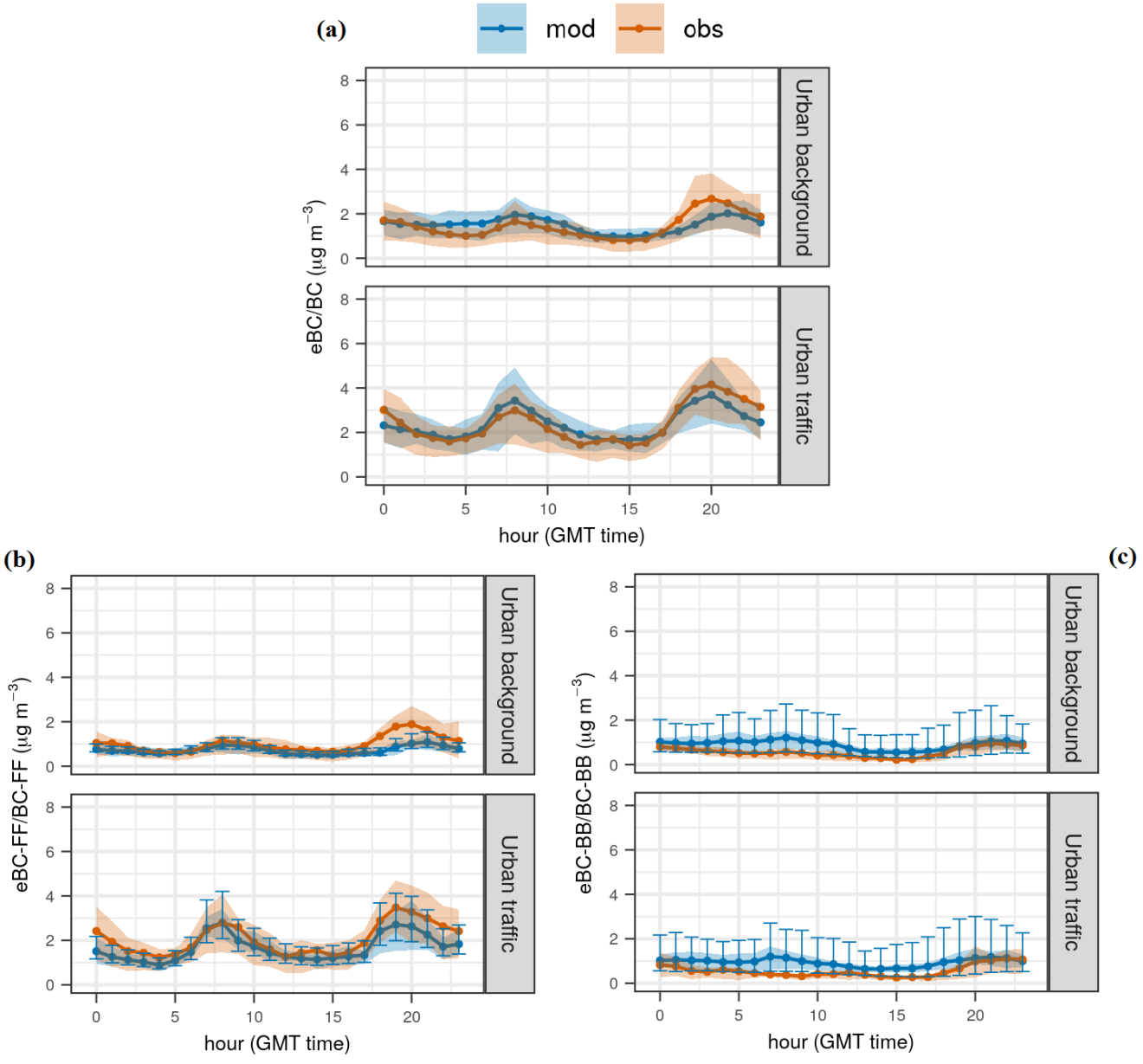

Figure 6. Comparative analysis of modelled (BC, blue) and observed (eBC, red) mean daily cycles during the first period for total BC concentrations (Panel a), Fossil Fuel-derived BC (Panel b), and Biomass Burning-derived BC (Panel c). The shaded regions in all three panels depict the interquartile range encompassing observations (red) and model outcomes (blue) for the base scenario. Error bars in Panels (b) and (c) delineate the minimum and maximum average concentrations derived from the simulated scenarios in this study. Dots correspond to average concentrations from the base case scenario.

https://doi.org/10.5194/egusphere-2023-2641
Preprint. Discussion started: 8 February 2024

When analysing the second period, a contrasting behaviour in the modelled concentrations is observed between the traffic and background sites (Figure 7, panel a). At the urban background station, the modelled concentrations are generally overestimated during most of the night and morning hours. However, the magnitude of the night peak is well captured, albeit with a one hour delay. On the other hand, the measured concentrations at the traffic site are consistently underestimated during every hour of the day, although the hourly trend is well represented by the hybrid modelling system.

Despite the divergent results observed at the two stations, it's important to bear in mind that the concentrations represented at the two stations refer to two different periods: measurements were carried out from 26 December 2020 to 7 January 2021 at the urban background site and from 26 December 2020 to 21 January 2021 at the urban traffic site. Therefore, these data sets are not directly comparable (see previous explanations in this section).

Looking more closely at the contributions of individual sources to the total eBC/BC concentrations at the urban background site, a detailed examination shows that the overestimation in the morning peak is due to an overestimation of biomass burning emissions (Figure 7, panel c), which is consistent with the results of the first period. Conversely, the night peak is well captured by the average concentration derived from all biomass burning scenarios considered. The modelled BC-FF concentrations, although showing very limited variability throughout the day, are in good agreement with the measurements, suggesting that a precise modulation of traffic and other fossil fuel related sources for holidays (which predominantly characterise most days of the campaign at the background site) could have been applied.

At the traffic site, biomass burning concentrations are well simulated by the modelling system, with observations closely matching the averaged concentrations from all simulated scenarios for most hours, except for the morning peak, confirming the previously developed hypothesis. In more detail, the results of the second period suggest a more plausible scenario where a single daily peak occurs at night between 20:00 and 22:00 GMT. Moreover, the daily modulation profile based on the concept of heating degree days seems to be quite effective in consistently reproducing biomass emissions for domestic heating under different winter temperatures (see Figures S2 and S3). The modelled BC concentrations originating from fossil fuels at the traffic site show a tendency to converge towards the upper limits of the error bars corresponding to the upper range of the BC/PM speciation factors recommended by the EEA, i.e. by the combination of the TRF-exh-3, TRF-nexh-3 and TRF-bck-3 scenarios. While this result might suggest that the upper range of the speciation factors might reflect the composition of the vehicle fleet in Modena, we believe that the source of this underestimation is mainly related to the difficulties encountered by the modelling system in simulating specific meteorological events and the presence of emitting sources that pose challenges to the simulation.

As discussed earlier, instead of a consistent underestimation of the observed trend throughout the simulated period due to low speciation factors, distinct episodes of significant underestimation can be identified (see Figure 5). These episodes were characterised by either robust meteorological stagnation (such as the events of 13-14 June and 18-19 June 2021) or the likely presence of sporadic high-emitting sources in the vicinity of the traffic station (such as on 3 January 2021), which the modelling system was unable to capture. To support the hypothesis of inaccuracies in the simulation of the pronounced atmospheric stability observed on 13-14 and on 18-19 January 2021, Figure S9 in the supplementary material provides an overview of the hourly simulated Planetary Boundary Layer (PBL) height by GRAL in Modena, a critical variable for vertical mixing

https://doi.org/10.5194/egusphere-2023-2641
Preprint. Discussion started: 8 February 2024

and pollutant dispersion. Although a direct comparison with measured values within Modena is not possible due to a lack of measurements, it is evident that the diurnal PBL height for the mentioned critical days (13-14 and 18-19 January 2021) is close to or even higher than that of the previous days, without any particular trend towards lower values. Consequently, the vertical dispersion of BC emitted at the city scale on these days was somewhat overestimated. Despite these inherent limitations, the results obtained from both the first and second periods show that the method used to estimate fossil fuel emissions, especially those from traffic, has proved its effectiveness in accurately reproducing the observed trend.

https://doi.org/10.5194/egusphere-2023-2641
Preprint. Discussion started: 8 February 2024

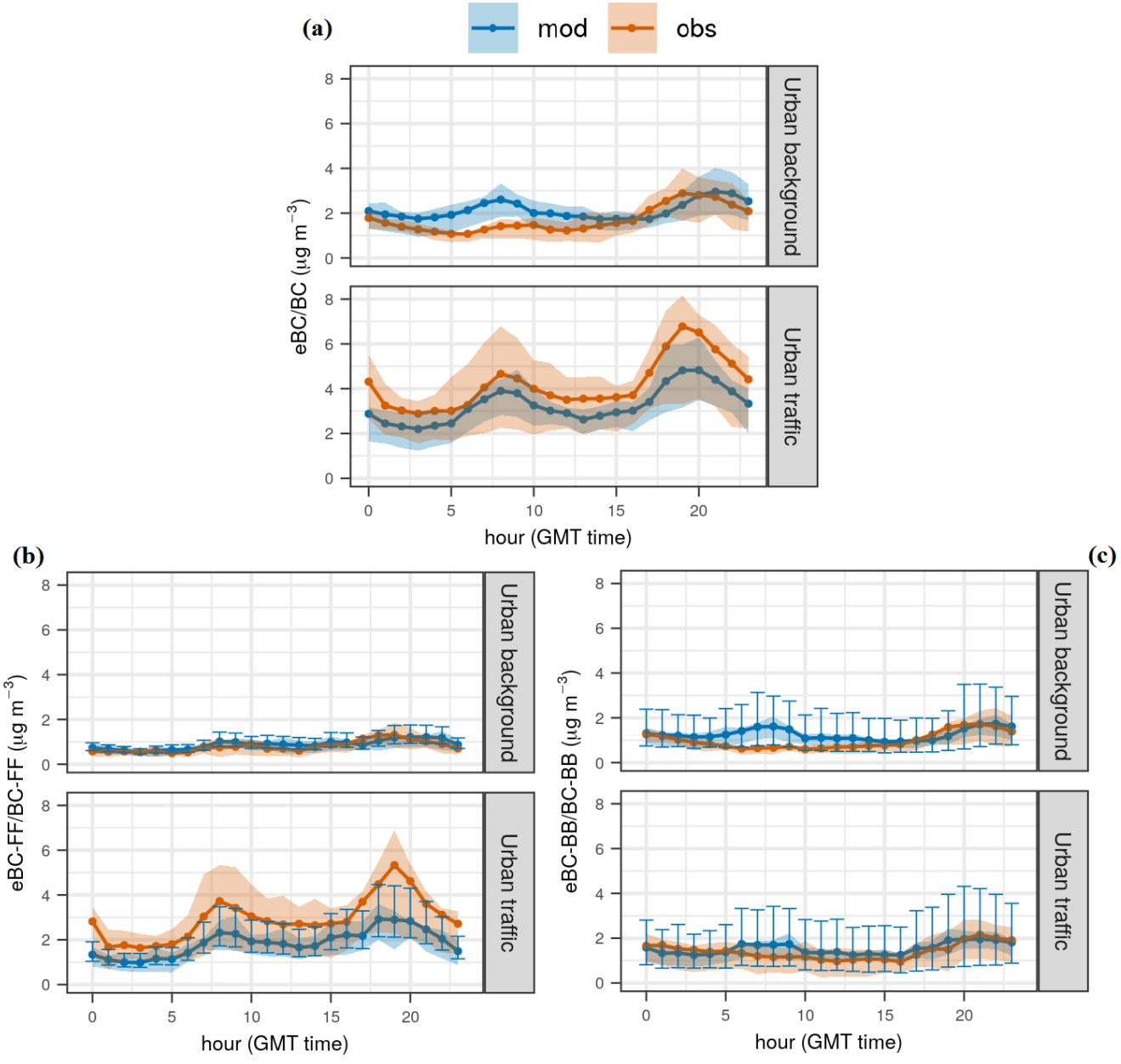

Figure 7. Comparative analysis of modelled (BC, blue) and observed (eBC, red) mean daily cycles during the second period for total BC concentrations (Panel a), Fossil Fuel-derived BC (Panel b), and Biomass Burning-derived BC (Panel c). The shaded regions in all three panels depict the interquartile range encompassing observations (red) and model outcomes (blue). Error bars in Panels (b) and (c) delineate the minimum and maximum average concentrations derived from the simulated scenarios in this study. Dots correspond to average concentrations from the base case scenario.

https://doi.org/10.5194/egusphere-2023-2641
Preprint. Discussion started: 8 February 2024

4.2.3 Dispersion modelling based source apportionment

Once the robustness of the hybrid modelling system in reproducing the observed trends was verified, the second phase of the study employed the same system to identify potential sources influencing urban BC concentrations in Modena. The design of the modelling framework allows a direct distinction between contributions originating from within the city (labelled as City in the Figures 8 and 9) and from sources located outside the urban area (labelled as bck in the Figures 8 and 9). This distinction is achieved through adjustments made to the CHIMERE code, enabling real-time apportionment for non-reactive BC. In addition, the ability of the Lagrangian model GRAL to store concentration fields for selected sources, allow direct apportionment of different urban emission sectors.

Figure 8 shows the average spatial contributions from each simulated source, which were calculated by analysing hourly maps from both the first and second simulated periods. In panel (a) of this figure, the upper facets show the average contributions of BB, FF, traffic non-exhaust and resuspension emissions from urban sources (labelled as City). Meanwhile, the lower facets show the average contributions from the same sources, but originating from areas outside the region of interest and transported over longer distances (labelled as bck).

When focusing on the contributions originating from within the city, these maps underscore the significant impact of BB on the overall levels of BC, as evident in the top-left facet of panel (a). Indeed, even though BC emissions are potentially absent or extremely low within the historical city centre, concentrations tend to spike in the surrounding area, reaching up to 2 $\mu g\,m^{-3}$ only from this contribution. This can be ascribed to the increasing density and height of buildings as one moves from rural areas into the historical centre. These factors give rise to intricate urban canyons that foster atmospheric stagnation, thereby hindering the dispersion and dilution of pollutants. Regarding FF contributions from urban sources (centre top-left facet of panel a), it is evident that traffic is the primary source of FF combustion, as indicated by the concentration peaks of BC. These peaks exhibit noticeable high spatial gradients, particularly prominent in streets characterised by heavy traffic, such as the urban ring road encircling the urban area, the small section of highway in the bottom-left corner of the domain and several other bustling urban streets. Furthermore, non-exhaust emissions and resuspension (respectively centre top-right and top-right facets of panel (a) also make a notable contribution to total BC concentrations, even if their absolute values are lower compared to those of BB and FF, especially in the vicinity of the aforementioned heavily trafficked streets.

In the lower facets of panel (a), the contributions from long-range transport are displayed. Although these maps show more uniform concentration patterns when compared with those at the city scale, BB concentrations remain the dominant contributor among the four source categories considered here. This underscores that emissions outside the urban centre also exert a noteworthy influence on urban BC concentrations. On the other hand, panel (b) of Figure 8 represents the sum of each single contribution from panel (a). This plot displays the capability of the hybrid modelling system in simulating urban concentration gradients originating from different source locations and it also underscores the ability of the Lagrangian modelling suite to reconstruct the impact of urban canyons, which play a crucial role in the accumulation of pollutants in the most critical areas of the city centre.

https://doi.org/10.5194/egusphere-2023-2641
Preprint. Discussion started: 8 February 2024

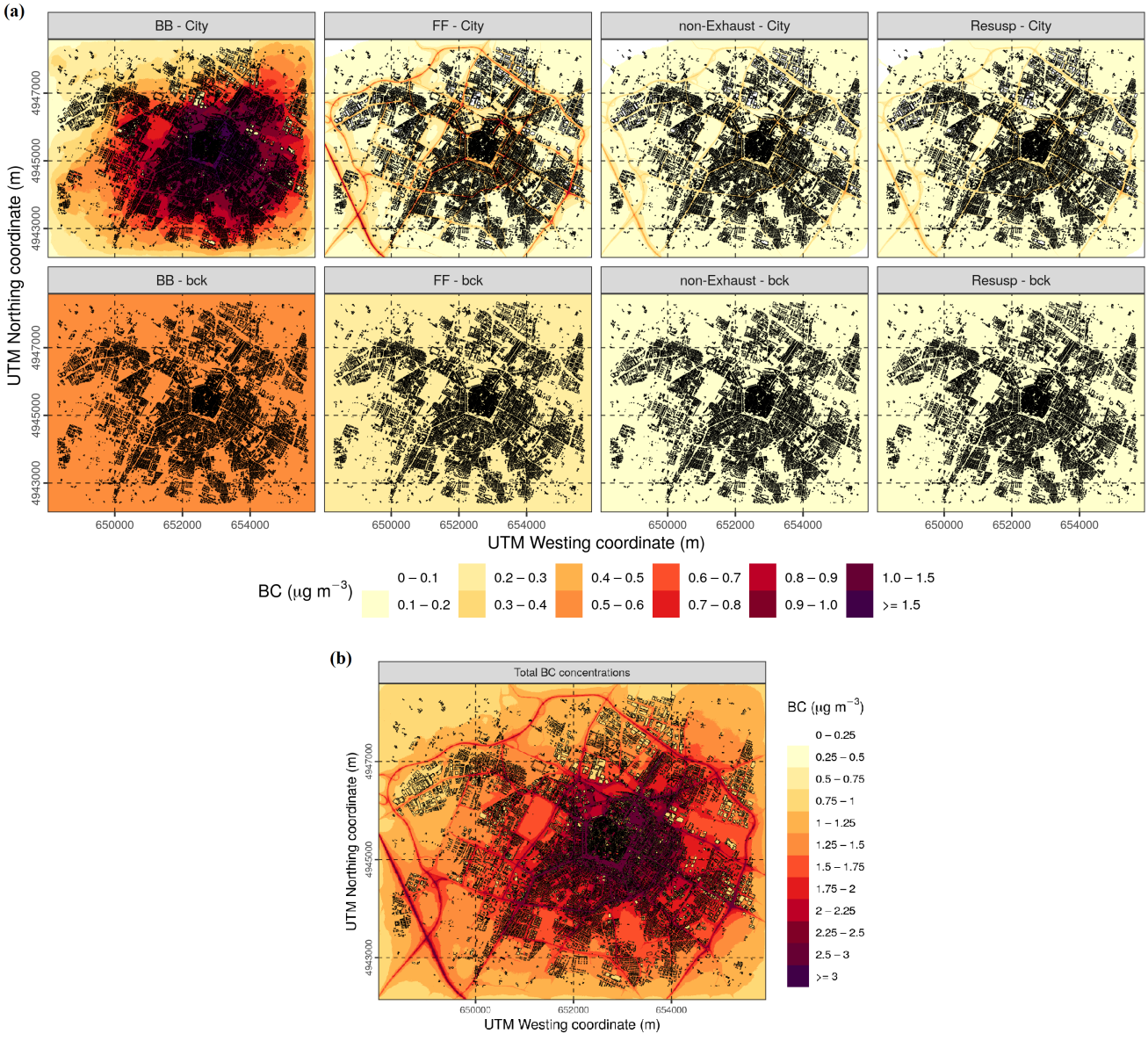

Figure 8. Modelled breakdown of BC contributions, differentiating between fossil fuels (FF), biomass burning (BB), traffic non-exhaust emissions and resuspension (panel a). The upper facets represent the BC contributions from local sources within the city (City), while the lower facets depict contributions from sources located outside the urban area (bck). Panel (b) displays the total average BC concentrations, accounting for contributions from all these sources. Black rectangles in the plots represent buildings. Please note the different scales used for panel (a) and panel (b).

Based on the results presented in Figure 8 and considering a receptor location equivalent in scale to the GRAL simulation domain, the average concentration over all cells in this area was calculated for all emission sources analysed here. The results

https://doi.org/10.5194/egusphere-2023-2641
Preprint. Discussion started: 8 February 2024

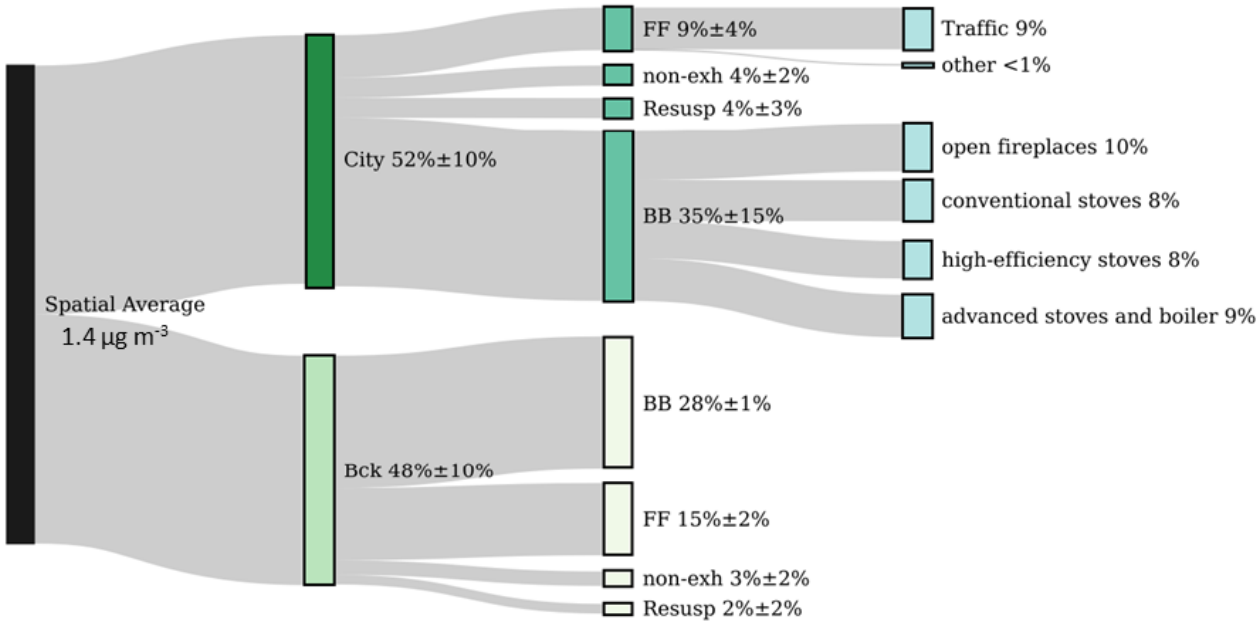

Figure 9. Sankey plot showing the percentage distribution of BC concentrations by source area and emission category.

indicate that the urban contribution accounts for 52% ± 10% of the total average BC concentration, while background sources contribute approximately 48% ± 10% to the local concentrations. A more detailed breakdown of the local urban contribution shows that BB accounts for 35% ± 15%, FF for 9% ± 4%, non-exhaust emissions for 4% ± 2% and resuspension for 4% ± 3%. It's also worth noting that FF is mainly attributed to traffic sources, with other FF sources accounting for less than 1%. In contrast, according to the Arpae local emission inventory, total BB emissions are roughly evenly distributed among open fireplaces (10%), conventional stoves (8%), high-efficiency stoves (8%), and advanced stoves and boilers (9%). Since there was no available data for a more detailed distribution of these emissions, we applied a consistent approach to spatially allocate all BB sources. As a result, the simulated BC concentrations align with the same percentage breakdown as the emission inventory. As for long-range transport, it contributes 28% ± 1% to BB emissions, 15% ± 2% to FF emissions, 3% ± 2% to non-exhaust emissions and 2% ± 2% to resuspension emissions. A summary of these percentages is given in the Sankey diagram presented in Figure 9.

The availability of detailed data on the composition of the circulating fleet, traffic volume and vehicle specific emission factors allows a more detailed examination of the total traffic contribution. Specifically, when traffic emissions are summed up, 50% can be attributed to exhaust emissions, while the remaining 50% is equally divided between non-exhaust and resuspension emissions, each contributing 25%. Looking at exhaust emissions in more detail, passenger cars (PC) are the main contributor, accounting for 35% of total transport emissions, while mopeds and motorcycles, light commercial vehicles, buses and trucks contribute 3%, 10% and 2% respectively. In addition, Euro 4 diesel passenger cars are responsible for the largest share of

https://doi.org/10.5194/egusphere-2023-2641
Preprint. Discussion started: 8 February 2024

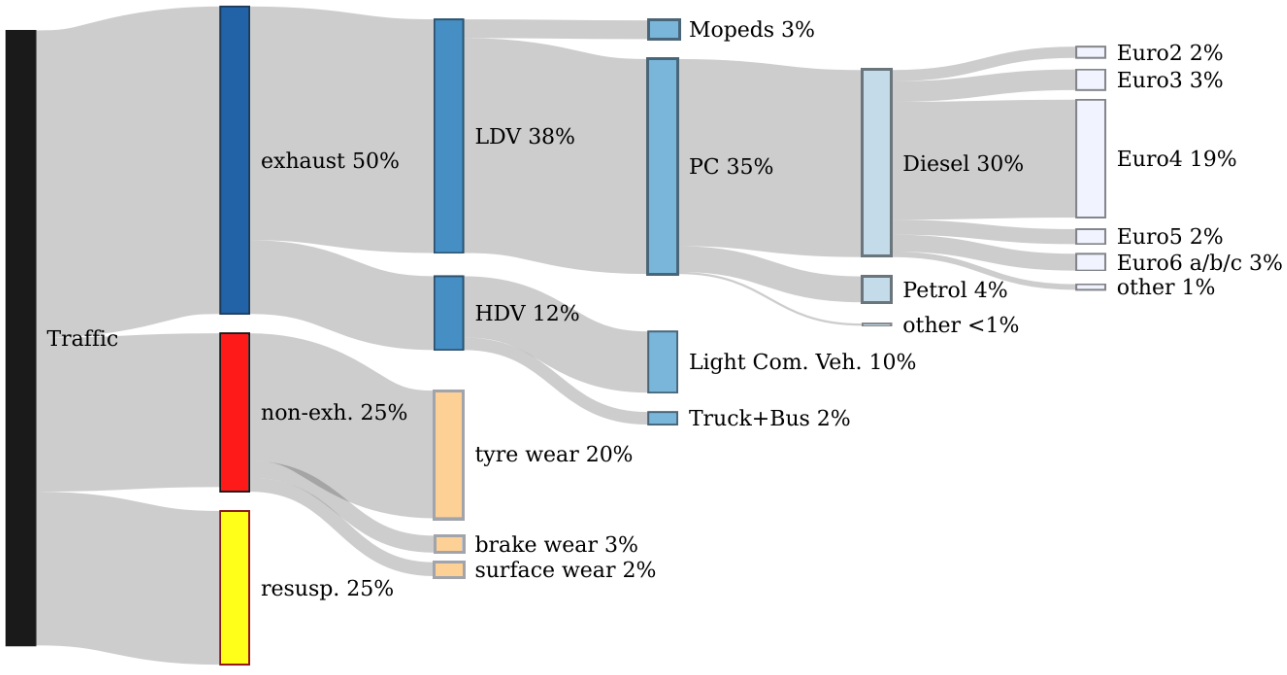

Figure 10. Sankey diagram illustrating the percentage distribution of BC emissions from urban traffic sources.

BC emissions in the urban environment, accounting for 19% of total transport emissions. This is due to their predominance in the vehicle composition (15% of the total fleet) and their associated emission factors. Detailed information on the local fleet composition and BC emission factors for the diesel and petrol PC categories can be found in Figures S11 and S12 in the supplement. On the other hand, BC emissions from tyre wear dominate the non-exhaust contribution, accounting for 20% of total traffic emissions, while brake wear and road wear emissions contribute 2% and 3% respectively. While these percentages represent emissions, it is important to note that all traffic emissions were consistently distributed over the same road areas and BC was treated as inert in the simulation. Consequently, the simulated BC concentrations closely match the percentages observed in the emission data. A summary of the percentage distribution of traffic emissions for the urban contribution can be found in the Sankey diagram shown in Figure 10.

5 Conclusions

The present article discusses the outcomes of an integrated modelling and measurement approach designed to assess black carbon (BC) levels and sources in Modena, a city located in the Po valley and chosen as representative of a typical medium-sized urban setting of the region. The eBC measurements were performed with two multi-wavelength micro-aethalometers of the Aethlabs MA200 series during two winter periods: the first from 4 February to 7 March 2020, and the second from 26 December 2020 to 21 January 2021, at two different urban sites. One site was selected to represent typical urban background

https://doi.org/10.5194/egusphere-2023-2641
Preprint. Discussion started: 8 February 2024

conditions, while the other was specifically chosen to capture high traffic intensity. In parallel to the measurement campaign, we implemented a hybrid modelling approach integrating the NINFA modelling suite (built upon the chemical transport model CHIMERE) with the Lagrangian model GRAMM-GRAL. This approach aimed to provide spatially resolved insights into BC concentrations and to identify potential sources contributing to BC levels in the urban environment of Modena. GRAMM-GRAL was used to reconstruct BC concentration fields at high resolution (4 m), taking into account local sources and the presence of obstacles (e.g. buildings, bridges or portals) in the flow field reconstruction. Conversely, NINFA was used to estimate the influence of external sources within the urban environment of Modena on BC concentrations.

Absorptions estimated with the MA200 instruments were further partitioned using the Multi-Wavelength Absorption Analyser (MWAA) model, allowing the distinction between different components, namely FF (emitted from fossil fuel sources), BB (from biomass burning) and BrC (brown carbon). The same partitioning was also used to differentiate eBC concentrations between fossil fuels (eBC-FF) and biomass combustion (eBC-BB). The absorption related to BrC showed a consistent and remarkably low presence throughout the day in both periods (around 0.5 Mm^{-1} in the first, 1.2 Mm^{-1} in the second). On the other hand, FF, a marker for traffic-related emissions, showed distinct diurnal peaks during rush hours, in the morning (07:00-08:00 GMT) and in the evening (18:00-20:00 GMT) for both periods, with values up to 187.2 Mm^{-1} (corresponding to 18.5 $\mu\mathrm{g\,m}^{-3}$ of eBC-FF concentration) at the urban traffic site. In contrast, BB showed less diurnal variability, with a minimum in the early afternoon (15:00-17:00 GMT) and a peak in the evening (20:00-21:00 GMT), and generally lower absorption compared to FF. A comparison of the two seasons showed significant differences. The period from 26 December 2020 to 21 January 2021 had higher FF and BB concentrations, likely due to different meteorological conditions such as lower wind speeds and increased atmospheric stability, leading to frequent thermal inversions and a higher frequency of stable atmospheric conditions. In addition, lower temperatures likely led to more biomass burning for heating, which increased eBC concentrations.

In the second part of the study, the concentrations reproduced by the hybrid modelling system were compared with the observations recorded by the MA200 instruments. During the period from 4 February to 7 March 2020, the hybrid system showed a robust performance, with an MB of 0.02 $\mu\mathrm{g\,m}^{-3}$ (+2%) at the urban background site and -0.12 $\mu\mathrm{g\,m}^{-3}$ (-5%) at the traffic site. The linear correlation coefficients were 0.51 and 0.62 respectively. Importantly, the daily concentration peaks were consistently captured even under varying meteorological conditions, including periods of high wind speed. However, during the period from 26 December 2020 to 21 January 2021, a contrasting behaviour was observed between the traffic and background stations. At the urban background site, measurements were only available for the period from 26 December 2020 to 7 January 2021, which included 7 holidays out of 13 measurement days. Under these conditions, the model showed a tendency to overestimate concentrations from biomass burning emissions, especially during the early part of the day. This effect was similar to that observed in the first period, but more pronounced due to the increased influence of the holidays. For this station the MB increased to 0.25 $\mu\mathrm{g\,m}^{-3}$ (+15%) and the correlation coefficient decreased to 0.38. Conversely, measurements at the traffic station covered the entire period from 26 December 2020 to 21 January 2021. Throughout this period, the meteorological conditions were favourable for the accumulation of pollutants, characterised by the presence of high pressure systems and thermal inversions. In such circumstances, the model struggled to fully capture the complex meteorological dynamics, leading to a notable reduction in the mean bias (-0.92 $\mu\mathrm{g\,m}^{-3}$, -22%) and correlation coefficient (0.34). In addition, the presence of

https://doi.org/10.5194/egusphere-2023-2641
Preprint. Discussion started: 8 February 2024

occasional high emission sources in close proximity to the traffic monitoring site may have contributed to increased eBC concentrations. Despite the decrease in performance during the second period, the statistical metrics considered in this evaluation, including FAC2, NAD, FB and NMSE, met the established acceptance criteria for urban dispersion modelling. Furthermore, these results are consistent with metrics from similar studies simulating BC concentrations in urban areas.

The same system was used to identify the impact of different sources on the spatial average BC concentrations, both inside and outside the urban area of Modena. The analysis showed that the city itself contributes to 52% ± 10% of the total average BC concentration, while background sources account for about 48% ± 10% of the local concentrations. A detailed breakdown of the city's contribution showed that BB is responsible for 35% ± 15%, FF for 9% ± 4%, non-exhaust emissions for 4% ± 2% and resuspension for 4% ± 3%. In particular, FF is mainly attributed to traffic sources, with other FF sources playing a negligible role. On the other hand, BB emissions are evenly distributed between open fireplaces, conventional stoves, high efficiency stoves and advanced stoves, as detailed in the Arpae local emission inventory. As for long-distance transport, it contributes 28% ± 1% to BB emissions, 15% ± 2% to FF emissions, 3% ± 2% to non-exhaust emissions and 2% ± 2% to resuspension emissions. Finally, when analysing the traffic-related concentrations, we found that 50% can be attributed to exhaust emissions (in particular 19% of the total for Euro4, diesel passenger cars), with the remaining 50% divided equally between non-exhaust and resuspension sources, each contributing 25%. In future developments, this research can serve as a valuable basis for more comprehensive air quality management strategies in Modena and similar medium-sized urban areas in the Po Valley. Ongoing monitoring and assessment of BC concentrations, together with a deeper understanding of the sources contributing to BC levels, can provide valuable insights for policy makers and urban planners seeking to reduce the impact of BC on air quality and public health in the region.

Appendix A: Symbol and acronyms

https://doi.org/10.5194/egusphere-2023-2641
Preprint. Discussion started: 8 February 2024

Table A1. Description of symbols and acronyms used in the text.

Symbol	Description
α	Absorption Ångström exponent
b_{abs}	Aerosol absorption coefficient
$b_{abs,BC}^{BB}$	b_{abs} from BC by biomass burning
$b_{abs,BC}^{FF}$	b_{abs} from BC by fossil fuel combustion
b_{abs}^{BrC}	b_{abs} from brown carbon
BB	Biomass burning
BC	Black carbon
BrC	Brown carbon
CCN	Cloud condensation nuclei
C_{ref}	multi-scattering correction factor
CTMs	Chemical Transport Models
EC	Elemental Carbon
EEA	European Environmental Agency
EF	Emission Factor
FF	Fossil fuel
IN	Ice nuclei
IR	Infrared
MAAP	Multi-angle absorption photometers
MAE	Mass absorption efficiency
MWAA	Multi-wavelength absorption analyser
NMVOCs	Non-methane volatile organic compounds
PBL	Planetary boundary layer
PC	Passenger cars
PM	Particulate matter
PTFE	Polytetrafluoroethylene
RB	Rural background
SNAP	Selected nomenclature for air pollution
UB	Urban background
UT	Urban traffic
UV	Ultraviolet
WHO	World health organization

https://doi.org/10.5194/egusphere-2023-2641
Preprint. Discussion started: 8 February 2024

Code and data availability. The source code for CHIMERE, GRAMM-GRAL and the emission model VERT used in this study will be released at Zenodo in case of publication. Raw *in-situ* aerosol absorption data from MA200 devices for Modena during the study period is available at https://doi.org/10.5281/zenodo.8140250, last access: November 6, 2023) (Bigi, 2023, version 1.0.0).

Author contributions. GV designed the study in collaboration with AB, performed the CHIMERE and GRAMM-GRAL simulations, and wrote the paper. AB acquired the funds for the micro-athalomter measurements, performed the measurement campaigns and provided support in the data analysis. MS, ST, and GG provided essential resources and contributed to data interpretation. All co-authors review, commented and contributed to the manuscript.

Competing interests. The authors declare no competing interests.

Acknowledgements. This study was supported by the project 'Black Air' (CUP E94I19001080005) funded by the University of Modena and Reggio Emilia and the *Fondazione di Modena* under the programme "Fondo di Ateneo per la Ricerca 2019". This work has also been partially funded by the European Union—NextGenerationEU under the ECOSISTER Project—Spoke 4 (CUP E93C22001100001). Carla Barbieri and Enrica Canossa from ARPAE are kindly acknowledged for hosting the micro-aethalomters in the air quality monitoring stations and for granting full access to these sites. We would like to extend our appreciation to Dario Massabò and Vera Bernardoni for the application of the MWAA model to micro-aethalomters measurements used in this study. The municipality of Modena is also kindly acknowledged for providing the vehicular traffic data.

https://doi.org/10.5194/egusphere-2023-2641
Preprint. Discussion started: 8 February 2024

References

ACI: Autoritratto, http://www.aci.it/laci/studi-e-ricerche/dati-e-statistiche/autoritratto.html, 2023.

Aethlabs: Tech. rep., https://help.aethlabs.com/s/article/Define-Specific-Attenuation-Cross-section-%CF%83ATN-or-Sigma-Value-for-the-microAeth-MA-Series-instruments, 2024.

Alas, H. D. C., Müller, T., Weinhold, K., Pfeifer, S., Glojek, K., Gregorič, A., Močnik, G., Drinovec, L., Costabile, F., Ristorini, M., and Wiedensohler, A.: Performance of microAethalometers: Real-world Field Intercomparisons from Multiple Mobile Measurement Campaigns in Different Atmospheric Environments, Aerosol and Air Quality Research, 20, 2640–2653, https://doi.org/10.4209/aaqr.2020.03.0113, publisher: Taiwan Association for Aerosol Research, 2020.

Ali, M. U., Siyi, L., Yousaf, B., Abbas, Q., Hameed, R., Zheng, C., Kuang, X., and Wong, M. H.: Emission sources and full spectrum of health impacts of black carbon associated polycyclic aromatic hydrocarbons (PAHs) in urban environment: A review, Critical Reviews in Environmental Science and Technology, 51, 857–896, https://doi.org/10.1080/10643389.2020.1738854, publisher: Taylor & Francis _eprint: https://doi.org/10.1080/10643389.2020.1738854, 2021.

Almbauer, R., Pucher, K., and Sturm, P. J.: Air quality modeling for the city of Graz, Meteorology and Atmospheric Physics, 57, 31–42, https://doi.org/10.1007/BF01044152, 1995.

Amato, F., Karanasiou, A., Moreno, T., Alastuey, A., Orza, J. A. G., Lumbreras, J., Borge, R., Boldo, E., Linares, C., and Querol, X.: Emission factors from road dust resuspension in a Mediterranean freeway, Atmospheric Environment, 61, 580–587, https://doi.org/10.1016/j.atmosenv.2012.07.065, 2012.

Bauer, J. J., Yu, X.-Y., Cary, R., Laulainen, N., and Berkowitz, C.: Characterization of the Sunset Semi-Continuous Carbon Aerosol Analyzer, Journal of the Air & Waste Management Association, 59, 826–833, https://doi.org/10.3155/1047-3289.59.7.826, publisher: Taylor & Francis _eprint: https://doi.org/10.3155/1047-3289.59.7.826, 2009.

Belis, C. A., Pikridas, M., Lucarelli, F., Petralia, E., Cavalli, F., Calzolai, G., Berico, M., and Sciare, J.: Source apportionment of fine PM by combining high time resolution organic and inorganic chemical composition datasets, Atmospheric Environment: X, 3, 100 046, https://doi.org/10.1016/j.aeaoa.2019.100046, 2019.

Berchet, A., Zink, K., Muller, C., Oettl, D., Brunner, J., Emmenegger, L., and Brunner, D.: A cost-effective method for simulating city-wide air flow and pollutant dispersion at building resolving scale, Atmospheric Environment, 158, 181–196, https://doi.org/10.1016/j.atmosenv.2017.03.030, 2017.

Bernardoni, V., Vecchi, R., Valli, G., Piazzalunga, A., and Fermo, P.: PM10 source apportionment in Milan (Italy) using time-resolved data, Science of The Total Environment, 409, 4788–4795, https://doi.org/10.1016/j.scitotenv.2011.07.048, 2011.

Bernardoni, V., Elser, M., Valli, G., Valentini, S., Bigi, A., Fermo, P., Piazzalunga, A., and Vecchi, R.: Size-segregated aerosol in a hot-spot pollution urban area: Chemical composition and three-way source apportionment, Environmental Pollution, 231, 601–611, https://doi.org/10.1016/j.envpol.2017.08.040, 2017a.

Bernardoni, V., Pileci, R. E., Caponi, L., and Massabò, D.: The Multi-Wavelength Absorption Analyzer (MWAA) Model as a Tool for Source and Component Apportionment Based on Aerosol Absorption Properties: Application to Samples Collected in Different Environments, Atmosphere, 8, 218, https://doi.org/10.3390/atmos8110218, number: 11 Publisher: Multidisciplinary Digital Publishing Institute, 2017b.

Bernardoni, V., Ferrero, L., Bolzacchini, E., Forello, A. C., Gregorič, A., Massabò, D., Močnik, G., Prati, P., Rigler, M., Santagostini, L., Soldan, F., Valentini, S., Valli, G., and Vecchi, R.: Determination of Aethalometer multiple-scattering enhancement parameters and

https://doi.org/10.5194/egusphere-2023-2641
Preprint. Discussion started: 8 February 2024

impact on source apportionment during the winter 2017/18 EMEP/ACTRIS/COLOSSAL campaign in Milan, Atmospheric Measurement Techniques, 14, 2919–2940, https://doi.org/10.5194/amt-14-2919-2021, publisher: Copernicus GmbH, 2021.

Bigi, A. and Ghermandi, G.: Trends and variability of atmospheric $PM_{2.5}$ and $PM_{10–2.5}$ concentration in the Po Valley, Italy, Atmospheric Chemistry and Physics, 16, 15 777–15 788, https://doi.org/https://doi.org/10.5194/acp-16-15777-2016, 2016.

Bigi, A., Ghermandi, G., and Harrison, R. M.: Analysis of the air pollution climate at a background site in the Po valley, Journal of Environmental Monitoring, 14, 552–563, https://doi.org/10.1039/C1EM10728C, 2012.

Bigi, A., Bianchi, F., De Gennaro, G., Di Gilio, A., Fermo, P., Ghermandi, G., Prévôt, A. S. H., Urbani, M., Valli, G., Vecchi, R., and Piazzalunga, A.: Hourly composition of gas and particle phase pollutants at a central urban background site in Milan, Italy, Atmospheric Research, 186, 83–94, https://doi.org/10.1016/j.atmosres.2016.10.025, 2017.

Bigi, A., Veratti, G., Andrews, E., Collaud Coen, M., Guerrieri, L., Bernardoni, V., Massabò, D., Ferrero, L., Teggi, S., and Ghermandi, G.: Aerosol absorption using in situ filter-based photometers and ground-based sun photometry in the Po Valley urban atmosphere, Atmospheric Chemistry and Physics, 23, 14 841–14 869, https://doi.org/10.5194/acp-23-14841-2023, publisher: Copernicus GmbH, 2023.

Bond, T. C., Doherty, S. J., Fahey, D. W., Forster, P. M., Berntsen, T., DeAngelo, B. J., Flanner, M. G., Ghan, S., Kärcher, B., Koch, D., Kinne, S., Kondo, Y., Quinn, P. K., Sarofim, M. C., Schultz, M. G., Schulz, M., Venkataraman, C., Zhang, H., Zhang, S., Bellouin, N., Guttikunda, S. K., Hopke, P. K., Jacobson, M. Z., Kaiser, J. W., Klimont, Z., Lohmann, U., Schwarz, J. P., Shindell, D., Storelvmo, T., Warren, S. G., and Zender, C. S.: Bounding the role of black carbon in the climate system: A scientific assessment, Journal of Geophysical Research: Atmospheres, 118, 5380–5552, https://doi.org/10.1002/jgrd.50171, _eprint: https://onlinelibrary.wiley.com/doi/pdf/10.1002/jgrd.50171, 2013.

Brasseur, O., Declerck, P., Heene, B., and Vanderstraeten, P.: Modelling Black Carbon concentrations in two busy street canyons in Brussels using CANSBC, Atmospheric Environment, 101, 72–81, https://doi.org/10.1016/j.atmosenv.2014.10.049, 2015.

Brown, S., Minor, H., O'Brien, T., Hameed, Y., Feenstra, B., Kuebler, D., Wetherell, W., Day, R., Tun, R., Landis, E., and Rice, J.: Review of Sunset OC/EC Instrument Measurements During the EPA's Sunset Carbon Evaluation Project, Atmosphere, 10, 287, https://doi.org/10.3390/atmos10050287, number: 5 Publisher: Multidisciplinary Digital Publishing Institute, 2019.

CCL: CORINE Land Cover, https://land.copernicus.eu/en/products/corine-land-cover, 2018.

Chan, T. W., Brook, J. R., Smallwood, G. J., and Lu, G.: Time-resolved measurements of black carbon light absorption enhancement in urban and near-urban locations of southern Ontario, Canada, Atmospheric Chemistry and Physics, 11, 10 407–10 432, https://doi.org/10.5194/acp-11-10407-2011, publisher: Copernicus GmbH, 2011.

Chang, C.-Y., You, R., Armstrong, D., Bandi, A., Cheng, Y.-T., Burkhardt, P. M., Becerra-Dominguez, L., Madison, M. C., Tung, H.-Y., Zeng, Z., Wu, Y., Song, L., Phillips, P. E., Porter, P., Knight, J. M., Putluri, N., Yuan, X., Marcano, D. C., McHugh, E. A., Tour, J. M., Catic, A., Maneix, L., Burt, B. M., Lee, H.-S., Corry, D. B., and Kheradmand, F.: Chronic exposure to carbon black ultrafine particles reprograms macrophage metabolism and accelerates lung cancer, Science Advances, 8, eabq0615, https://doi.org/10.1126/sciadv.abq0615, 2022.

Cherian, R., Quaas, J., Salzmann, M., and Tomassini, L.: Black carbon indirect radiative effects in a climate model, 69, 1369 342, https://doi.org/10.1080/16000889.2017.1369342, number: 1 Publisher: Stockholm University Press, 2017.

Chow, J. C., Watson, J. G., Chen, L.-W. A., Chang, M. O., Robinson, N. F., Trimble, D., and Kohl, S.: The IMPROVE_A Temperature Protocol for Thermal/Optical Carbon Analysis: Maintaining Consistency with a Long-Term Database, Journal of the Air & Waste Management Association, 57, 1014–1023, https://doi.org/10.3155/1047-3289.57.9.1014, publisher: Taylor & Francis _eprint: https://doi.org/10.3155/1047-3289.57.9.1014, 2007.

https://doi.org/10.5194/egusphere-2023-2641
Preprint. Discussion started: 8 February 2024

Chung, S. H. and Seinfeld, J. H.: Climate response of direct radiative forcing of anthropogenic black carbon, Journal of Geophysical Research: Atmospheres, 110, https://doi.org/10.1029/2004JD005441, _eprint: https://onlinelibrary.wiley.com/doi/pdf/10.1029/2004JD005441, 2005.

Clima, A. E. S. I. M.: LIBSIM, https://github.com/ARPA-SIMC/libsim, original-date: 2015-10-01T12:34:51Z, 2023.

Costabile, F., Gilardoni, S., Barnaba, F., Di Ianni, A., Di Liberto, L., Dionisi, D., Manigrasso, M., Paglione, M., Poluzzi, V., Rinaldi, M., Facchini, M. C., and Gobbi, G. P.: Characteristics of brown carbon in the urban Po Valley atmosphere, Atmospheric Chemistry and Physics, 17, 313–326, https://doi.org/10.5194/acp-17-313-2017, publisher: Copernicus GmbH, 2017.

Curci, G., Alyuz, U., Barò, R., Bianconi, R., Bieser, J., Christensen, J. H., Colette, A., Farrow, A., Francis, X., Jiménez-Guerrero, P., Im, U., Liu, P., Manders, A., Palacios-Peña, L., Prank, M., Pozzoli, L., Sokhi, R., Solazzo, E., Tuccella, P., Unal, A., Vivanco, M. G., Hogrefe, C., and Galmarini, S.: Modelling black carbon absorption of solar radiation: combining external and internal mixing assumptions, Atmospheric Chemistry and Physics, 19, 181–204, https://doi.org/10.5194/acp-19-181-2019, publisher: Copernicus GmbH, 2019.

Denby, B. R., Sundvor, I., Johansson, C., Pirjola, L., Ketzel, M., Norman, M., Kupiainen, K., Gustafsson, M., Blomqvist, G., Kauhaniemi, M., and Omstedt, G.: A coupled road dust and surface moisture model to predict non-exhaust road traffic induced particle emissions (NORTRIP). Part 2: Surface moisture and salt impact modelling, Atmospheric Environment, 81, 485–503, https://doi.org/10.1016/j.atmosenv.2013.09.003, 2013.

Drinovec, L., Močnik, G., Zotter, P., Prévôt, A. S. H., Ruckstuhl, C., Coz, E., Rupakheti, M., Sciare, J., Müller, T., Wiedensohler, A., and Hansen, A. D. A.: The "dual-spot" Aethalometer: an improved measurement of aerosol black carbon with real-time loading compensation, Atmospheric Measurement Techniques, 8, 1965–1979, https://doi.org/10.5194/amt-8-1965-2015, publisher: Copernicus GmbH, 2015.

Drinovec, L., Jagodič, U., Pirker, L., Škarabot, M., Kurtjak, M., Vidović, K., Ferrero, L., Visser, B., Röhrbein, J., Weingartner, E., Kalbermatter, D. M., Vasilatou, K., Bühlmann, T., Pascale, C., Müller, T., Wiedensohler, A., and Močnik, G.: A dual-wavelength photothermal aerosol absorption monitor: design, calibration and performance, Atmospheric Measurement Techniques, 15, 3805–3825, https://doi.org/10.5194/amt-15-3805-2022, publisher: Copernicus GmbH, 2022.

EEA: The application of models under the European Union's Air Quality Directive: A technical reference guide — European Environment Agency, https://www.eea.europa.eu/publications/fairmode, 2011.

EEA: 1.A Combustion — European Environment Agency, https://www.eea.europa.eu/publications/emep-eea-guidebook-2019/part-b-sectoral-guidance-chapters/1-energy/1-a-combustion, 2019.

EPA: Document Display | NEPIS | US EPA, https://nepis.epa.gov/Exe/ZyNET.exe/2000D6B8.TXT?ZyActionD=ZyDocument&Client=EPA&Index=1995+Thru+1999&Docs=&Query=&Time=&EndTime=&SearchMethod=1&TocRestrict=n&Toc=&TocEntry=&QField=&QFieldYear=&QFieldMonth=&QFieldDay=&IntQFieldOp=0&ExtQFieldOp=0&XmlQuery=&File=D%3A%5Czyfiles%5CIndex%20Data%5C95thru99%5CTxt%5C00000016%5C2000D6B8.txt&User=ANONYMOUS&Password=anonymous&SortMethod=h%7C-&MaximumDocuments=1&FuzzyDegree=0&ImageQuality=r75g8/r75g8/x150y150g16/i425&Display=hpfr&DefSeekPage=x&SearchBack=ZyActionL&Back=ZyActionS&BackDesc=Results%20page&MaximumPages=1&ZyEntry=1&SeekPage=x&ZyPURL, 2000.

European Council, .: On Ambient Air Quality and Cleaner Air for Europe 2008/50/EC, Off. J. Eur. Union, 1, 1–44, https://eur-lex.europa.eu/legal-content/EN/TXT/PDF/?uri=CELEX:32008L0050&from=en, 2008.

Ferrero, L., Močnik, G., Cogliati, S., Gregorič, A., Colombo, R., and Bolzacchini, E.: Heating Rate of Light Absorbing Aerosols: Time-Resolved Measurements, the Role of Clouds, and Source Identification, Environmental Science & Technology, 52, 3546–3555, https://doi.org/10.1021/acs.est.7b04320, publisher: American Chemical Society, 2018.

https://doi.org/10.5194/egusphere-2023-2641
Preprint. Discussion started: 8 February 2024

Ferrero, L., Bernardoni, V., Santagostini, L., Cogliati, S., Soldan, F., Valentini, S., Massabò, D., Močnik, G., Gregorič, A., Rigler, M., Prati, P., Bigogno, A., Losi, N., Valli, G., Vecchi, R., and Bolzacchini, E.: Consistent determination of the heating rate of light-absorbing aerosol using wavelength- and time-dependent Aethalometer multiple-scattering correction, Science of The Total Environment, 791, 148 277, https://doi.org/10.1016/j.scitotenv.2021.148277, 2021.

Fischer, D. A. and Smith, G. D.: A portable, four-wavelength, single-cell photoacoustic spectrometer for ambient aerosol absorption, Aerosol Science and Technology, 52, 393–406, https://doi.org/10.1080/02786826.2017.1413231, publisher: Taylor & Francis _eprint: https://doi.org/10.1080/02786826.2017.1413231, 2018.

Forello, A. C., Bernardoni, V., Calzolai, G., Lucarelli, F., Massabò, D., Nava, S., Pileci, R. E., Prati, P., Valentini, S., Valli, G., and Vecchi, R.: Exploiting multi-wavelength aerosol absorption coefficients in a multi-time resolution source apportionment study to retrieve source-dependent absorption parameters, Atmospheric Chemistry and Physics, 19, 11 235–11 252, https://doi.org/10.5194/acp-19-11235-2019, publisher: Copernicus GmbH, 2019.

Geoportale-Emilia-Romagna: Homepage, https://geoportale.regione.emilia-romagna.it, 2023.

Ghermandi, G., Fabbi, S., Arvani, B., Veratti, G., Bigi, A., and Teggi, S.: Impact Assessment of Pollutant Emissions in the Atmosphere from a Power Plant over a Complex Terrain and under Unsteady Winds, Sustainability, 9, 2076, https://doi.org/10.3390/su9112076, number: 11 Publisher: Multidisciplinary Digital Publishing Institute, 2017.

Ghermandi, G., Fabbi, S., Bigi, A., Veratti, G., Despini, F., Teggi, S., Barbieri, C., and Torreggiani, L.: Impact assessment of vehicular exhaust emissions by microscale simulation using automatic traffic flow measurements, Atmospheric Pollution Research, 10, 1473–1481, https://doi.org/10.1016/j.apr.2019.04.004, 2019.

Ghermandi, G., Fabbi, S., Veratti, G., Bigi, A., and Teggi, S.: Estimate of Secondary NO2 Levels at Two Urban Traffic Sites Using Observations and Modelling, Sustainability, 12, 7897, https://doi.org/10.3390/su12197897, 2020.

Gilardoni, S., Massoli, P., Marinoni, A., Mazzoleni, C., Freedman, A., Lonati, G., Iuliis, S. D., and Gianelle, V.: Spatial and Temporal Variability of Carbonaceous Aerosol Absorption in the Po Valley, Aerosol and Air Quality Research, 20, 2624–2639, https://doi.org/10.4209/aaqr.2020.03.0085, publisher: Taiwan Association for Aerosol Research, 2020.

Grahame, T. J., Klemm, R., and Schlesinger, R. B.: Public health and components of particulate matter: the changing assessment of black carbon, Journal of the Air & Waste Management Association (1995), 64, 620–660, https://doi.org/10.1080/10962247.2014.912692, 2014.

Grange, S. K., Lötscher, H., Fischer, A., Emmenegger, L., and Hueglin, C.: Evaluation of equivalent black carbon source apportionment using observations from Switzerland between 2008 and 2018, Atmospheric Measurement Techniques, 13, 1867–1885, https://doi.org/10.5194/amt-13-1867-2020, publisher: Copernicus GmbH, 2020.

Guevara, M., Tena, C., Porquet, M., Jorba, O., and Pérez García-Pando, C.: HERMESv3, a stand-alone multi-scale atmospheric emission modelling framework – Part 2: The bottom–up module, Geoscientific Model Development, 13, 873–903, https://doi.org/10.5194/gmd-13-873-2020, publisher: Copernicus GmbH, 2020.

Guo, X., Nakayama, T., Yamada, H., Inomata, S., Tonokura, K., and Matsumi, Y.: Measurement of the light absorbing properties of diesel exhaust particles using a three-wavelength photoacoustic spectrometer, Atmospheric Environment, 94, 428–437, https://doi.org/10.1016/j.atmosenv.2014.05.042, 2014.

Hanna, S. and Chang, J.: Acceptance criteria for urban dispersion model evaluation, Meteorology and Atmospheric Physics, 116, 133–146, https://doi.org/10.1007/s00703-011-0177-1, 2012.

https://doi.org/10.5194/egusphere-2023-2641
Preprint. Discussion started: 8 February 2024

Helin, A., Niemi, J. V., Virkkula, A., Pirjola, L., Teinilä, K., Backman, J., Aurela, M., Saarikoski, S., Rönkkö, T., Asmi, E., and Timonen, H.: Characteristics and source apportionment of black carbon in the Helsinki metropolitan area, Finland, Atmospheric Environment, 190, 87–98, https://doi.org/10.1016/j.atmosenv.2018.07.022, 2018.

Hendricks, J., Kärcher, B., and Lohmann, U.: Effects of ice nuclei on cirrus clouds in a global climate model, Journal of Geophysical Research: Atmospheres, 116, https://doi.org/10.1029/2010JD015302, _eprint: https://onlinelibrary.wiley.com/doi/pdf/10.1029/2010JD015302, 2011.

Henzing, J. S., Olivié, D. J. L., and van Velthoven, P. F. J.: A parameterization of size resolved below cloud scavenging of aerosols by rain, Atmospheric Chemistry and Physics, 6, 3363–3375, https://doi.org/10.5194/acp-6-3363-2006, publisher: Copernicus GmbH, 2006.

INEMAR: Inventario regionale emissioni in atmosfera (INEMAR) - Dati Arpae, https://dati.arpae.it/dataset/inventario-emissioni-aria-inemar, 2023.

ISPRA: Inventario Nazionale – EMISSIONI, https://emissioni.sina.isprambiente.it/inventario-nazionale/.

Janssen, N. A., Gerlofs-Nijland, M. E., Lanki, T., Salonen, R. O., Cassee, F., Hoek, G., Fischer, P., Brunekreef, B., and Krzyzanowski, M.: Health effects of black carbon, World Health Organization. Regional Office for Europe, https://apps.who.int/iris/handle/10665/352615, 2012.

Janssen, N. A. H., Hoek, G., Simic-Lawson, M., Fischer, P., van Bree, L., ten Brink, H., Keuken, M., Atkinson, R. W., Anderson, H. R., Brunekreef, B., and Cassee, F. R.: Black carbon as an additional indicator of the adverse health effects of airborne particles compared with PM10 and PM2.5, Environmental Health Perspectives, 119, 1691–1699, https://doi.org/10.1289/ehp.1003369, 2011.

Ježek, I., Blond, N., Skupinski, G., and Močnik, G.: The traffic emission-dispersion model for a Central-European city agrees with measured black carbon apportioned to traffic, Atmospheric Environment, 184, 177–190, https://doi.org/10.1016/j.atmosenv.2018.04.028, 2018.

Kaskaoutis, D. G., Grivas, G., Stavroulas, I., Bougiatioti, A., Liakakou, E., Dumka, U. C., Gerasopoulos, E., and Mihalopoulos, N.: Apportionment of black and brown carbon spectral absorption sources in the urban environment of Athens, Greece, during winter, Science of The Total Environment, 801, 149 739, https://doi.org/10.1016/j.scitotenv.2021.149739, 2021a.

Kaskaoutis, D. G., Grivas, G., Stavroulas, I., Liakakou, E., Dumka, U. C., Gerasopoulos, E., and Mihalopoulos, N.: Effect of aerosol types from various sources at an urban location on spectral curvature of scattering and absorption coefficients, Atmospheric Research, 264, 105 865, https://doi.org/10.1016/j.atmosres.2021.105865, 2021b.

Koch, D., Balkanski, Y., Bauer, S. E., Easter, R. C., Ferrachat, S., Ghan, S. J., Hoose, C., Iversen, T., Kirkevåg, A., Kristjansson, J. E., Liu, X., Lohmann, U., Menon, S., Quaas, J., Schulz, M., Seland, , Takemura, T., and Yan, N.: Soot microphysical effects on liquid clouds, a multi-model investigation, Atmospheric Chemistry and Physics, 11, 1051–1064, https://doi.org/10.5194/acp-11-1051-2011, publisher: Copernicus GmbH, 2011.

Lee, J. and Moosmüller, H.: Measurement of Light Absorbing Aerosols with Folded-Jamin Photothermal Interferometry, Sensors, 20, 2615, https://doi.org/10.3390/s20092615, number: 9 Publisher: Multidisciplinary Digital Publishing Institute, 2020.

Li, B., Wang, Y., and Li, Z.: A method for monitoring mass concentration of black carbon particulate matter using photothermal interferometry, Environmental Science and Pollution Research, 23, 4692–4699, https://doi.org/10.1007/s11356-015-5702-1, 2016.

Li, C., Windwer, E., Fang, Z., Nissenbaum, D., and Rudich, Y.: Correcting micro-aethalometer absorption measurements for brown carbon aerosol, Science of The Total Environment, 777, 146 143, https://doi.org/10.1016/j.scitotenv.2021.146143, 2021.

Liakakou, E., Stavroulas, I., Kaskaoutis, D. G., Grivas, G., Paraskevopoulou, D., Dumka, U. C., Tsagkaraki, M., Bougiatioti, A., Oikonomou, K., Sciare, J., Gerasopoulos, E., and Mihalopoulos, N.: Long-term variability, source apportionment and spectral properties of black carbon

https://doi.org/10.5194/egusphere-2023-2641
Preprint. Discussion started: 8 February 2024

at an urban background site in Athens, Greece, Atmospheric Environment, 222, 117 137, https://doi.org/10.1016/j.atmosenv.2019.117137, 2020.

Liu, C., Chung, C. E., Yin, Y., and Schnaiter, M.: The absorption Ångström exponent of black carbon: from numerical aspects, Atmospheric Chemistry and Physics, 18, 6259–6273, https://doi.org/10.5194/acp-18-6259-2018, publisher: Copernicus GmbH, 2018.

Lonati, G., Ozgen, S., Ripamonti, G., and Signorini, S.: Variability of Black Carbon and Ultrafine Particle Concentration on Urban Bike Routes in a Mid-Sized City in the Po Valley (Northern Italy), Atmosphere, 8, 40, https://doi.org/10.3390/atmos8020040, number: 2 Publisher: Multidisciplinary Digital Publishing Institute, 2017.

Lugon, L., Vigneron, J., Debert, C., Chrétien, O., and Sartelet, K.: Black carbon modeling in urban areas: investigating the influence of resuspension and non-exhaust emissions in streets using the Street-in-Grid model for inert particles (SinG-inert), Geoscientific Model Development, 14, 7001–7019, https://doi.org/10.5194/gmd-14-7001-2021, publisher: Copernicus GmbH, 2021.

Mailler, S., Menut, L., Khvorostyanov, D., Valari, M., Couvidat, F., Siour, G., Turquety, S., Briant, R., Tuccella, P., Bessagnet, B., Colette, A., Létinois, L., Markakis, K., and Meleux, F.: CHIMERE-2017: from urban to hemispheric chemistry-transport modeling, Geoscientific Model Development, 10, 2397–2423, https://doi.org/10.5194/gmd-10-2397-2017, publisher: Copernicus GmbH, 2017.

Massabò, D., Caponi, L., Bernardoni, V., Bove, M. C., Brotto, P., Calzolai, G., Cassola, F., Chiari, M., Fedi, M. E., Fermo, P., Giannoni, M., Lucarelli, F., Nava, S., Piazzalunga, A., Valli, G., Vecchi, R., and Prati, P.: Multi-wavelength optical determination of black and brown carbon in atmospheric aerosols, Atmospheric Environment, 108, 1–12, https://doi.org/10.1016/j.atmosenv.2015.02.058, 2015.

Mbengue, S., Zikova, N., Schwarz, J., Vodička, P., Šmejkalová, A. H., and Holoubek, I.: Mass absorption cross-section and absorption enhancement from long term black and elemental carbon measurements: A rural background station in Central Europe, Science of The Total Environment, 794, 148 365, https://doi.org/10.1016/j.scitotenv.2021.148365, 2021.

Menon, S., Hansen, J., Nazarenko, L., and Luo, Y.: Climate Effects of Black Carbon Aerosols in China and India, Science, 297, 2250–2253, https://doi.org/10.1126/science.1075159, publisher: American Association for the Advancement of Science, 2002.

Menut, L., Bessagnet, B., Briant, R., Cholakian, A., Couvidat, F., Mailler, S., Pennel, R., Siour, G., Tuccella, P., Turquety, S., and Valari, M.: The CHIMERE v2020r1 online chemistry-transport model, Geoscientific Model Development, 14, 6781–6811, https://doi.org/10.5194/gmd-14-6781-2021, publisher: Copernicus GmbH, 2021.

Merico, E., Cesari, D., Dinoi, A., Gambaro, A., Barbaro, E., Guascito, M. R., Giannossa, L. C., Mangone, A., and Contini, D.: Intercomparison of carbon content in PM10 and PM2.5 measured with two thermo-optical protocols on samples collected in a Mediterranean site, Environmental Science and Pollution Research, 26, 29 334–29 350, https://doi.org/10.1007/s11356-019-06117-7, 2019.

Minderytė, A., Pauraite, J., Dudoitis, V., Plauškaitė, K., Kilikevičius, A., Matijošius, J., Rimkus, A., Kilikevičienė, K., Vainorius, D., and Byčenkienė, S.: Carbonaceous aerosol source apportionment and assessment of transport-related pollution, Atmospheric Environment, 279, 119 043, https://doi.org/10.1016/j.atmosenv.2022.119043, 2022.

Mircea, M., Bessagnet, B., D'Isidoro, M., Pirovano, G., Aksoyoglu, S., Ciarelli, G., Tsyro, S., Manders, A., Bieser, J., Stern, R., Vivanco, M. G., Cuvelier, C., Aas, W., Prévôt, A. S. H., Aulinger, A., Briganti, G., Calori, G., Cappelletti, A., Colette, A., Couvidat, F., Fagerli, H., Finardi, S., Kranenburg, R., Rouïl, L., Silibello, C., Spindler, G., Poulain, L., Herrmann, H., Jimenez, J. L., Day, D. A., Tiitta, P., and Carbone, S.: EURODELTA III exercise: An evaluation of air quality models' capacity to reproduce the carbonaceous aerosol, Atmospheric Environment: X, 2, 100 018, https://doi.org/10.1016/j.aeaoa.2019.100018, 2019.

Moosmüller, H., Chakrabarty, R. K., and Arnott, W. P.: Aerosol light absorption and its measurement: A review, Journal of Quantitative Spectroscopy and Radiative Transfer, 110, 844–878, https://doi.org/10.1016/j.jqsrt.2009.02.035, 2009.

https://doi.org/10.5194/egusphere-2023-2641
Preprint. Discussion started: 8 February 2024

Mousavi, A., Sowlat, M. H., Lovett, C., Rauber, M., Szidat, S., Boffi, R., Borgini, A., De Marco, C., Ruprecht, A. A., and Sioutas, C.: Source apportionment of black carbon (BC) from fossil fuel and biomass burning in metropolitan Milan, Italy, Atmospheric Environment, 203, 252–261, https://doi.org/10.1016/j.atmosenv.2019.02.009, 2019.

Mues, A., Kuenen, J., Hendriks, C., Manders, A., Segers, A., Scholz, Y., Hueglin, C., Builtjes, P., and Schaap, M.: Sensitivity of air pollution simulations with LOTOS-EUROS to the temporal distribution of anthropogenic emissions, Atmospheric Chemistry and Physics, 14, 939–955, https://doi.org/10.5194/acp-14-939-2014, publisher: Copernicus GmbH, 2014.

Ntziachristos, L. and Boulter, P.: 1.A.3.b.vi-vii Road tyre and brake wear 2019 — European Environment Agency, https://www.eea.europa.eu/publications/emep-eea-guidebook-2019/part-b-sectoral-guidance-chapters/1-energy/1-a-combustion/1-a-3-b-vi/view, 2019.

Ntziachristos, L. and Samaras, Z.: 1.A.3.b.i-iv Road transport 2019 — European Environment Agency, https://www.eea.europa.eu/publications/emep-eea-guidebook-2019/part-b-sectoral-guidance-chapters/1-energy/1-a-combustion/1-a-3-b-i/view, 2019.

Oettl, D.: Evaluation of the Revised Lagrangian Particle Model GRAL Against Wind-Tunnel and Field Observations in the Presence of Obstacles, Boundary-Layer Meteorology, 155, 271–287, https://doi.org/10.1007/s10546-014-9993-4, 2015a.

Oettl, D.: A multiscale modelling methodology applicable for regulatory purposes taking into account effects of complex terrain and buildings on pollutant dispersion: a case study for an inner Alpine basin, Environmental Science and Pollution Research, 22, 17 860–17 875, https://doi.org/10.1007/s11356-015-4966-9, 2015b.

Oettl, D.: Quality assurance of the prognostic, microscale wind-field model GRAL 14.8 using wind-tunnel data provided by the German VDI guideline 3783-9, Journal of Wind Engineering and Industrial Aerodynamics, 142, 104–110, https://doi.org/10.1016/j.jweia.2015.03.014, 2015c.

Oettl, D.: Development of the Mesoscale Model GRAMM-SCI: Evaluation of Simulated Highly-Resolved Flow Fields in an Alpine and Pre-Alpine Region, Atmosphere, 12, 298, https://doi.org/10.3390/atmos12030298, number: 3 Publisher: Multidisciplinary Digital Publishing Institute, 2021.

Oettl, D. and Reifeltshammer, R.: Recent developments in high-resolution wind field modeling in complex terrain for dispersion simulations using GRAMM-SCI, Air Quality, Atmosphere & Health, https://doi.org/10.1007/s11869-023-01403-3, 2023.

Oettl, D. and Veratti, G.: A comparative study of mesoscale flow-field modelling in an Eastern Alpine region using WRF and GRAMM-SCI, Atmospheric Research, 249, 105 288, https://doi.org/10.1016/j.atmosres.2020.105288, 2021.

Paglione, M., Gilardoni, S., Rinaldi, M., Decesari, S., Zanca, N., Sandrini, S., Giulianelli, L., Bacco, D., Ferrari, S., Poluzzi, V., Scotto, F., Trentini, A., Poulain, L., Herrmann, H., Wiedensohler, A., Canonaco, F., Prévôt, A. S. H., Massoli, P., Carbone, C., Facchini, M. C., and Fuzzi, S.: The impact of biomass burning and aqueous-phase processing on air quality: a multi-year source apportionment study in the Po Valley, Italy, Atmospheric Chemistry and Physics, 20, 1233–1254, https://doi.org/10.5194/acp-20-1233-2020, publisher: Copernicus GmbH, 2020.

Pandolfo, J. P.: Motions with Inertial and Diurnal Period, Journal of Marine Research, 1969.

Pani, S. K., Wang, S.-H., Lin, N.-H., Chantara, S., Lee, C.-T., and Thepnuan, D.: Black carbon over an urban atmosphere in northern peninsular Southeast Asia: Characteristics, source apportionment, and associated health risks, Environmental Pollution, 259, 113 871, https://doi.org/10.1016/j.envpol.2019.113871, 2020.

Pepe, N., Pirovano, G., Balzarini, A., Toppetti, A., Riva, G. M., Amato, F., and Lonati, G.: Enhanced CAMx source apportionment analysis at an urban receptor in Milan based on source categories and emission regions, Atmospheric Environment: X, 2, 100 020, https://doi.org/10.1016/j.aeaoa.2019.100020, 2019.

https://doi.org/10.5194/egusphere-2023-2641
Preprint. Discussion started: 8 February 2024

Pernigotti, D., Georgieva, E., Thunis, P., and Bessagnet, B.: Impact of meteorology on air quality modeling over the Po valley in northern Italy, Atmospheric Environment, 51, 303–310, https://doi.org/10.1016/j.atmosenv.2011.12.059, 2012a.

Pernigotti, D., Georgieva, E., Thunis, P., Cuvelier, C., and de Meij, A.: The Impact of Meteorology on Air Quality Simulations over the Po Valley in Northern Italy, in: Air Pollution Modeling and its Application XXI, edited by Steyn, D. G. and Trini Castelli, S., NATO Science for Peace and Security Series C: Environmental Security, pp. 485–490, Springer Netherlands, Dordrecht, https://doi.org/10.1007/978-94-007-1359-8_81, 2012b.

Perrino, C., Catrambone, M., Dalla Torre, S., Rantica, E., Sargolini, T., and Canepari, S.: Seasonal variations in the chemical composition of particulate matter: a case study in the Po Valley. Part I: macro-components and mass closure, Environmental Science and Pollution Research, 21, 3999–4009, https://doi.org/10.1007/s11356-013-2067-1, 2014.

Petzold, A. and Niessner, R.: Photoacoustic soot sensor for in-situ black carbon monitoring, Applied Physics B, 63, 191–197, https://doi.org/10.1007/BF01095272, 1996.

Petzold, A., Ogren, J. A., Fiebig, M., Laj, P., Li, S.-M., Baltensperger, U., Holzer-Popp, T., Kinne, S., Pappalardo, G., Sugimoto, N., Wehrli, C., Wiedensohler, A., and Zhang, X.-Y.: Recommendations for reporting "black carbon" measurements, Atmospheric Chemistry and Physics, 13, 8365–8379, https://doi.org/10.5194/acp-13-8365-2013, publisher: Copernicus GmbH, 2013.

Ramanathan, V. and Carmichael, G.: Global and regional climate changes due to black carbon, Nature Geoscience, 1, 221–227, https://doi.org/10.1038/ngeo156, number: 4 Publisher: Nature Publishing Group, 2008.

Ramanathan, V., Crutzen, P. J., Kiehl, J. T., and Rosenfeld, D.: Aerosols, Climate, and the Hydrological Cycle, Science, 294, 2119–2124, https://doi.org/10.1126/science.1064034, publisher: American Association for the Advancement of Science, 2001.

Reche, C., Querol, X., Alastuey, A., Viana, M., Pey, J., Moreno, T., Rodríguez, S., González, Y., Fernández-Camacho, R., de la Rosa, J., Dall'Osto, M., Prévôt, A. S. H., Hueglin, C., Harrison, R. M., and Quincey, P.: New considerations for PM, Black Carbon and particle number concentration for air quality monitoring across different European cities, Atmospheric Chemistry and Physics, 11, 6207–6227, https://doi.org/10.5194/acp-11-6207-2011, publisher: Copernicus GmbH, 2011.

Roberts, D. L. and Jones, A.: Climate sensitivity to black carbon aerosol from fossil fuel combustion, Journal of Geophysical Research: Atmospheres, 109, https://doi.org/10.1029/2004JD004676, _eprint: https://onlinelibrary.wiley.com/doi/pdf/10.1029/2004JD004676, 2004.

Rohr, A. and McDonald, J.: Health effects of carbon-containing particulate matter: focus on sources and recent research program results, Critical Reviews in Toxicology, 46, 97–137, https://doi.org/10.3109/10408444.2015.1107024, 2016.

Sandradewi, J., Prévôt, A. S. H., Szidat, S., Perron, N., Alfarra, M. R., Lanz, V. A., Weingartner, E., and Baltensperger, U.: Using Aerosol Light Absorption Measurements for the Quantitative Determination of Wood Burning and Traffic Emission Contributions to Particulate Matter, Environmental Science & Technology, 42, 3316–3323, https://doi.org/10.1021/es702253m, publisher: American Chemical Society, 2008.

Saputra, D., Yoon, J.-h., Park, H., Heo, Y., Yang, H., Lee, E. J., Lee, S., Song, C.-W., and Lee, K.: Inhalation of Carbon Black Nanoparticles Aggravates Pulmonary Inflammation in Mice, Toxicological Research, 30, 83–90, https://doi.org/10.5487/TR.2014.30.2.083, 2014.

Savadkoohi, M., Pandolfi, M., Reche, C., Niemi, J. V., Mooibroek, D., Titos, G., Green, D. C., Tremper, A. H., Hueglin, C., Liakakou, E., Mihalopoulos, N., Stavroulas, I., Artiñano, B., Coz, E., Alados-Arboledas, L., Beddows, D., Riffault, V., De Brito, J. F., Bastian, S., Baudic, A., Colombi, C., Costabile, F., Chazeau, B., Marchand, N., Gómez-Amo, J. L., Estellés, V., Matos, V., van der Gaag, E., Gille, G., Luoma, K., Manninen, H. E., Norman, M., Silvergren, S., Petit, J.-E., Putaud, J.-P., Rattigan, O. V., Timonen, H., Tuch, T., Merkel, M., Weinhold, K., Vratolis, S., Vasilescu, J., Favez, O., Harrison, R. M., Laj, P., Wiedensohler, A., Hopke, P. K., Petäjä, T., Alastuey, A., and

https://doi.org/10.5194/egusphere-2023-2641
Preprint. Discussion started: 8 February 2024

Querol, X.: The variability of mass concentrations and source apportionment analysis of equivalent black carbon across urban Europe, Environment International, 178, 108 081, https://doi.org/10.1016/j.envint.2023.108081, 2023.

Scotto, F., Bacco, D., Lasagni, S., Trentini, A., Poluzzi, V., and Vecchi, R.: A multi-year source apportionment of PM2.5 at multiple sites in the southern Po Valley (Italy), Atmospheric Pollution Research, 12, 101 192, https://doi.org/10.1016/j.apr.2021.101192, 2021.

Segersson, D., Eneroth, K., Gidhagen, L., Johansson, C., Omstedt, G., Nylén, A. E., and Forsberg, B.: Health Impact of PM10, PM2.5 and Black Carbon Exposure Due to Different Source Sectors in Stockholm, Gothenburg and Umea, Sweden, International Journal of Environmental Research and Public Health, 14, 742, https://doi.org/10.3390/ijerph14070742, number: 7 Publisher: Multidisciplinary Digital Publishing Institute, 2017.

Singh, V., Ravindra, K., Sahu, L., and Sokhi, R.: Trends of atmospheric black carbon concentration over the United Kingdom, Atmospheric Environment, 178, 148–157, https://doi.org/10.1016/j.atmosenv.2018.01.030, 2018.

Skamarock, C., Klemp, B., Dudhia, J., Gill, O., Barker, D., Duda, G., Huang, X.-y., Wang, W., and Powers, G.: A Description of the Advanced Research WRF Version 3, https://doi.org/10.5065/D68S4MVH, 2008.

Song, X., Hu, Y., Ma, Y., Jiang, L., Wang, X., Shi, A., Zhao, J., Liu, Y., Liu, Y., Tang, J., Li, X., Zhang, X., Guo, Y., and Wang, S.: Is short-term and long-term exposure to black carbon associated with cardiovascular and respiratory diseases? A systematic review and meta-analysis based on evidence reliability, BMJ Open, 12, e049 516, https://doi.org/10.1136/bmjopen-2021-049516, publisher: British Medical Journal Publishing Group Section: Public health, 2022.

Stavroulas, I., Pikridas, M., Grivas, G., Bezantakos, S., Liakakou, E., Kalkavouras, P., Veratti, G., Bigi, A., Gerasopoulos, E., Sciare, J., and Mihalopoulos, N.: Field evaluation of miniature absorption photometers in an Eastern Mediterranean urban environment, 11th International Aerosol Conference (IAC 2022), Athens, Greece, 4-9 September 2022., 2022.

Stortini, M., Arvani, B., and Deserti, M.: Operational Forecast and Daily Assessment of the Air Quality in Italy: A Copernicus-CAMS Downstream Service, Atmosphere, 11, 447, https://doi.org/10.3390/atmos11050447, 2020.

Tang, J., Cheng, W., Gao, J., Li, Y., Yao, R., Rothman, N., Lan, Q., Campen, M. J., Zheng, Y., and Leng, S.: Occupational exposure to carbon black nanoparticles increases inflammatory vascular disease risk: an implication of an ex vivo biosensor assay, Particle and Fibre Toxicology, 17, 47, https://doi.org/10.1186/s12989-020-00378-8, 2020.

Thouron, L., Seigneur, C., Kim, Y., Mahé, F., André, M., Lejri, D., Villegas, D., Bruge, B., Chanut, H., and Pellan, Y.: Intercomparison of three modeling approaches for traffic-related road dust resuspension using two experimental data sets, Transportation Research Part D: Transport and Environment, 58, 108–121, https://doi.org/10.1016/j.trd.2017.11.003, 2018.

Thunis, P., Galmarini, S., Martilli, A., Clappier, A., Andronopoulos, S., Bartzis, J., Vlachogiannis, D., De Ridder, K., Moussiopoulos, N., Sahm, P., Almbauer, R., Sturm, P., Oettl, D., Dierer, S., and Schlünzen, K. H.: An inter-comparison exercise of mesoscale flow models applied to an ideal case simulation, Atmospheric Environment, 37, 363–382, https://doi.org/10.1016/S1352-2310(02)00888-9, 2003.

Thunis, P., Clappier, A., Beekmann, M., Putaud, J. P., Cuvelier, C., Madrazo, J., and de Meij, A.: Non-linear response of $PM_{2.5}$ to changes in NO_x and NH_3 emissions in the Po basin (Italy): consequences for air quality plans, Atmospheric Chemistry and Physics, 21, 9309–9327, https://doi.org/10.5194/acp-21-9309-2021, publisher: Copernicus GmbH, 2021.

Titos, G., del Águila, A., Cazorla, A., Lyamani, H., Casquero-Vera, J. A., Colombi, C., Cuccia, E., Gianelle, V., Močnik, G., Alastuey, A., Olmo, F. J., and Alados-Arboledas, L.: Spatial and temporal variability of carbonaceous aerosols: Assessing the impact of biomass burning in the urban environment, Science of The Total Environment, 578, 613–625, https://doi.org/10.1016/j.scitotenv.2016.11.007, 2017.

Tobler, A. K., Skiba, A., Canonaco, F., Močnik, G., Rai, P., Chen, G., Bartyzel, J., Zimnoch, M., Styszko, K., Nęcki, J., Furger, M., Różański, K., Baltensperger, U., Slowik, J. G., and Prevot, A. S. H.: Characterization of non-refractory (NR) PM_1 and source apportionment of

https://doi.org/10.5194/egusphere-2023-2641
Preprint. Discussion started: 8 February 2024

organic aerosol in Kraków, Poland, Atmospheric Chemistry and Physics, 21, 14 893–14 906, https://doi.org/10.5194/acp-21-14893-2021, publisher: Copernicus GmbH, 2021.

Troen, I. B. and Mahrt, L.: A simple model of the atmospheric boundary layer; sensitivity to surface evaporation, Boundary-Layer Meteorology, 37, 129–148, https://doi.org/10.1007/BF00122760, 1986.

Van Leer, B.: Towards the ultimate conservative difference scheme. IV. A new approach to numerical convection, Journal of Computational Physics, 23, 276–299, https://doi.org/10.1016/0021-9991(77)90095-X, 1977.

Vecchi, R., Bernardoni, V., Valentini, S., Piazzalunga, A., Fermo, P., and Valli, G.: Assessment of light extinction at a European polluted urban area during wintertime: Impact of PM1 composition and sources, Environmental Pollution, 233, 679–689, https://doi.org/10.1016/j.envpol.2017.10.059, 2018.

Veratti, G., Fabbi, S., Bigi, A., Lupascu, A., Tinarelli, G., Teggi, S., Brusasca, G., Butler, T. M., and Ghermandi, G.: Towards the coupling of a chemical transport model with a micro-scale Lagrangian modelling system for evaluation of urban NOx levels in a European hotspot, Atmospheric Environment, 223, 117 285, https://doi.org/10.1016/j.atmosenv.2020.117285, 2020.

Veratti, G., Bigi, A., Lupascu, A., Butler, T. M., and Ghermandi, G.: Urban population exposure forecast system to predict NO2 impact by a building-resolving multi-scale model approach, Atmospheric Environment, 261, 118 566, https://doi.org/10.1016/j.atmosenv.2021.118566, 2021.

Veratti, G., Stortini, M., Amorati, R., Bressan, L., Giovannini, G., Bande, S., Bissardella, F., Ghigo, S., Angelino, E., Colombo, L., Fossati, G., Malvestiti, G., Marongiu, A., Dalla Fontana, A., Intini, B., and Pillon, S.: Impact of NOx and NH3 Emission Reduction on Particulate Matter across Po Valley: A LIFE-IP-PREPAIR Study, Atmosphere, 14, 762, https://doi.org/10.3390/atmos14050762, number: 5 Publisher: Multidisciplinary Digital Publishing Institute, 2023.

Visser, B., Röhrbein, J., Steigmeier, P., Drinovec, L., Močnik, G., and Weingartner, E.: A single-beam photothermal interferometer for in situ measurements of aerosol light absorption, Atmospheric Measurement Techniques, 13, 7097–7111, https://doi.org/10.5194/amt-13-7097-2020, publisher: Copernicus GmbH, 2020.

Visser, B., Bilal, J., Flöry, N., Wipf, M., Steigmeier, P., Rüggeberg, T., Betschon, F., and Weingartner, E.: Waveguide based passively demodulated photothermal interferometer for light absorption measurements of trace substances, Applied Optics, 62, 374–384, https://doi.org/10.1364/AO.476868, publisher: Optica Publishing Group, 2023.

Vitali, L., Cuvelier, K., Piersanti, A., Monteiro, A., Adani, M., Amorati, R., Bartocha, A., D'Ausilio, A., Durka, P., Gama, C., Giovannini, G., Janssen, S., Przybyła, T., Stortini, M., Vranckx, S., and Thunis, P.: A standardized methodology for the validation of air quality forecast applications (F-MQO): lessons learnt from its application across Europe, Geoscientific Model Development, 16, 6029–6047, https://doi.org/10.5194/gmd-16-6029-2023, publisher: Copernicus GmbH, 2023.

Wang, C.: A modeling study on the climate impacts of black carbon aerosols, Journal of Geophysical Research: Atmospheres, 109, https://doi.org/10.1029/2003JD004084, _eprint: https://onlinelibrary.wiley.com/doi/pdf/10.1029/2003JD004084, 2004.

Wang, R., Balkanski, Y., Boucher, O., Ciais, P., Schuster, G. L., Chevallier, F., Samset, B. H., Liu, J., Piao, S., Valari, M., and Tao, S.: Estimation of global black carbon direct radiative forcing and its uncertainty constrained by observations, Journal of Geophysical Research: Atmospheres, 121, 5948–5971, https://doi.org/10.1002/2015JD024326, _eprint: https://onlinelibrary.wiley.com/doi/pdf/10.1002/2015JD024326, 2016.

WHO: Global air quality guidelines: particulate matter (PM2.5 and PM10), ozone, nitrogen dioxide, sulfur dioxide and carbon monoxide, World Health Organization, https://iris.who.int/handle/10665/345329, accepted: 2021-09-21T12:41:37Z, 2021.

https://doi.org/10.5194/egusphere-2023-2641
Preprint. Discussion started: 8 February 2024

Yus-Díez, J., Bernardoni, V., Močnik, G., Alastuey, A., Ciniglia, D., Ivančič, M., Querol, X., Perez, N., Reche, C., Rigler, M., Vecchi, R., Valentini, S., and Pandolfi, M.: Determination of the multiple-scattering correction factor and its cross-sensitivity to scattering and wavelength dependence for different AE33 Aethalometer filter tapes: a multi-instrumental approach, Atmospheric Measurement Techniques, 14, 6335–6355, https://doi.org/10.5194/amt-14-6335-2021, publisher: Copernicus GmbH, 2021.

Zhang, L., Gong, S., Padro, J., and Barrie, L.: A size-segregated particle dry deposition scheme for an atmospheric aerosol module, Atmospheric Environment, 35, 549–560, https://doi.org/10.1016/S1352-2310(00)00326-5, 2001.

Zotter, P., Herich, H., Gysel, M., El-Haddad, I., Zhang, Y., Močnik, G., Hüglin, C., Baltensperger, U., Szidat, S., and Prévôt, A. S. H.: Evaluation of the absorption Ångström exponents for traffic and wood burning in the Aethalometer-based source apportionment using radiocarbon measurements of ambient aerosol, Atmospheric Chemistry and Physics, 17, 4229–4249, https://doi.org/10.5194/acp-17-4229-2017, publisher: Copernicus GmbH, 2017.